ALTERATIONS IN CARDIAC CONTRACTILITY AND HEART RATE MEDIATED BY BONE LOADING

A THESIS IN

Cellular and Molecular Biology

Presented to the faculty of the University of
Missouri-Kansas City in partial fulfillment of
The requirements for the degree

MASTER OF SCIENCE

By

MARK A GRAY

Dual B.S., Missouri State University, 2018

Kansas City, Missouri
2022

ALTERATIONS IN CARDIAC CONTRACTILITY AND HEART RATE MEDIATED BY BONE LOADING

Mark A Gray, Candidate for the Master of Science Degree

University of Missouri-Kansas City, 2022

ABSTRACT

The skeleton is a dynamic organ in complex interplay with the other systems of the body and is highly responsive to input from the external environment. Increasingly, evidence is mounting that the skeleton is the source of endocrine factors which affect both long term cardiac outcomes and acute cardiac performance.

Some factors, like FGF23, have been shown to augment calcium handling in cardiomyocytes while at the same time being used clinically as a predictor of cardiomorbidity in, for example, chronic kidney disease patients. Other factors, such as osteocalcin, have been shown to be sufficient to elicit a type of cardiac stress response, even in adrenalectomized mice. The circulating levels of these and other bone-derived factors are known to respond to activity level and exercise. A major environmental input for the skeleton, especially during exercise, is movement-induced strain.

Media conditioned by MLO-Y4 osteocyte cell line culture under fluid flow sheer stress was used to model the acute effects of bone strain on the contraction magnitude and contraction rate of *ex vivo* Langendorf-perfused hearts. EKG was then used to measure cardiac parameters during tibial straining of anesthetized mice. A serum sample was collected after tibia strain and analyzed by LC/QToF MS. We found that MLO-Y4 conditioned media increased both the total

force and the peak force of Langendorf-perfused hearts by approximately 25%. Somewhat paradoxically, in anesthetized mice we found that a 2-minute tibia strain induced a decrease in heart rate and an increase in heart rate variability which began within seconds, peaked after approximately one minute, then returned to baseline by the time tibia loading ended. LC/QToF was able to identify a variety of serum factors in the strained mice, which produced clusters when principle component analysis was used. One factor, which was the only factor statistically elevated in all groups, was increased in all individuals and had a molecular weight corresponding to acetate.

The results obtained in this study strongly suggests that the skeleton, responding to exercise-like mechanical strain, has the potential to rapidly augment cardiac performance. This may have implications in exercise training as well as reduced-function settings, such as bedrest, and may shed additional light on the interplay between bone and heart health.

APPROVAL PAGE

The faculty listed below, appointed by the Dean of the School of Biological and Chemical Sciences, have examined a thesis title "Alterations in Cardiac Contractility and Heart Rate Mediated by Bone Loading", presented by Mark A Gray, candidate for the Master of Science degree and certify that in their opinion it is worthy of acceptance.

Supervisory Committee

Michael Wacker, Ph.D.
Department of Biomedical Sciences, UMKC School of Medicine

Mark Johnson, Ph.D.
Department of Oral and Craniofacial Sciences, UMKC School of Dentistry

Karen Bame, Ph.D.
UMKC School of Biological and Chemical Sciences

Tara Allen, Ph.D.
UMKC School of Biological and Chemical Sciences

CONTENTS

LIST OF ILLUSTRATIONS

Figure Page

LIST OF TABLES

Table Page

ACKNOWLEDGEMENTS

I would like to thank my committee chair and mentor, Dr. Michael Wacker, whose expertise, guidance, financial support, patience, and flexibility made this work possible. Likewise, this project would not have been completed without the knowledgeable support of Dr. Mark Johnson, nor would I have ever been able to meet Dr. Wacker and Dr. Johnson if not for the accommodation, support, and patience of Dr. Karen Bame who both guided me on this academic journey and let me find my own way. Just as importantly, without Dr. Tara Allen's advice and excellent lectures, I could not have linked the systems discussed here to the rest of the body; this knowledge would exist in a vacuum, which would be a great loss. Finally, I would like to acknowledge Julian Vallejo, Dr. Nuria Lara, Mark Dallas, Dr. William Gutheil, and Amar Sharma for their incomparable technical skills and merciless editing.

CHAPTER 1

INTRODUCTION

Increasingly, the skeleton is understood to be a dynamic organ system involved in diverse and distant physiological functions. It has been demonstrated that bone cells and the mineral components of the skeleton have roles in regulating glucose metabolism, lipid storage, testosterone level, kidney function, and neuronal development (Guntur & Rosen, 2012). Recent laboratory research and clinical studies also suggest that the skeleton plays a role in cardiac function, both acutely and long-term, in both young and old, and in both healthy individuals and during periods of physiological pathology (von Jeinsen et al., 2019, Fohtung et al., 2017, Berger et al., 2019). Clinically, decreased bone mineral density, independent of age and other factors, is associated with a statistically significant increase in the risk for heart failure (Fohtung et al., 2017). Many signaling factors potentially play a role. For example, serum FGF23 has been found to predict the 2-year survival curve of patients with chronic kidney failure (CKD), the mortality of which is predominantly driven by cardiovascular disease (Zhang et al., 2015). Persistently high FGF23 has been shown to induce left ventricular hypertrophy via the calcineurin/NFAT pathway (Faul et al., 2011). Relatedly, increased serum Sclerostin, another bone-derived factor, is correlated with increased pulse wave velocity (the velocity at which the blood pressure pulse propagates through the circulation) in dialysis patients (Stavrinou et al., 2019) and serum osteocalcin, a third factor released primarily by bone cells, is used as a predictor of cardiac pathophysiology in patients suffering from chronic kidney disease (CKD) (Kamińska et al., 2021). General low bone mass has shown to correlate, independent of age or activity level, to

increased risk of atherosclerosis, endothelial disfunction, and carotid thickness in an over-80 population (Campos-Staffico et al., 2020). Genetic studies of GPRC6A, an GPCR which responds to osteocalcin, show that double knockout mice missing this receptor in the skeleton, where it is highly expressed, and the heart, where it is moderately expressed, develop both osteopenia and heart disease at a young age (Moser & van der Eerden, 2019). Taken together the body of research seems to imply a close, multi-faceted relationship between skeletal function and cardiac function.

1.1Bone Anatomy

Observable anatomical appearance gives rise to four broad types of bone, each having a specialized function: short, flat, irregular, and long. Short bones, such as carpals and kneecap, are as wide as they are long. Flat bones, such as the skull and scapula, provide protection to the organs and medial attachment for limb muscles. The shape of irregular bones does not fit the other categories due to the very specialized function of these bones, for example the vertebrae and zygomatic bones. The long bones are located mainly in the limbs and are the main components of the skeleton that are involved in physical locomotion. The main bones of the leg include the femur and tibia in humans; in mice these bones are fused and referred to jointly as the tibia. The femur and tibia are classified as long bones because their width is less than their length (DeSaix & Johnson, 2013). At the ends of the femur and tibia are regions of higher metabolic activity called the epiphysis, while the central length of the bone is a less active region called the diaphysis (See Figure 1). Changes in the length of long bones is driven by growth hormone (GH) and Insulin-like Growth Factor (IGF) and manifests as the accrual of new ossification at the epiphysial plate, near the ends of the

bones. Adult changes in the diameter of bone in the region of the diaphysis is instigated primarily by the amount of sclerostin produced by proximal osteocytes.

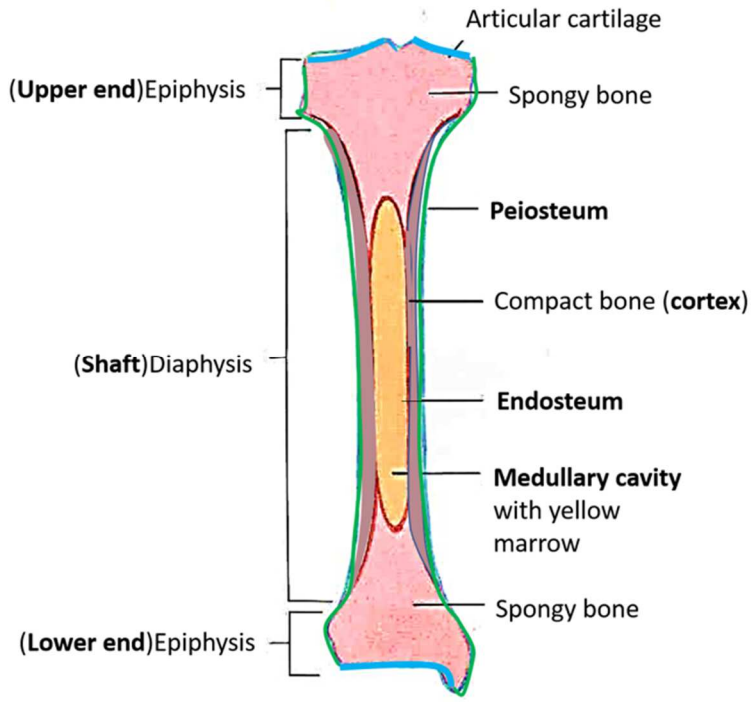

Figure 1. Diagram of the anatomy of a long bone. DeSaix, P and Johnson, E. (2013). *Anatomy and Physiology*. OpenStax. https://open.umn.edu/opentextbooks/textbooks/169

Externally, long bone is wrapped in a layer of connective tissue called the periosteum, except at the articular surfaces of joints (DeSaix & Johnson, 2013). The exterior of long bone is made up of a type of tissue called cortical (compact) bone, while the interior of long bone is made of cancellous (spongy) bone. Spongy bone contains bone marrow, located inside the medullary cavity. The medullary cavity is lined by the endosteum. The endosteum and periosteum, as vascular tissues, place the bone in broad contact with the circulatory system (Karner & Long, 2018).

The periosteum is dense, irregular connective tissue with an outer fibrous layer and an inner cambium layer (DeSaix & Johnson, 2013). The cambium supplies nutrients to the bone and is nociceptive, in contrast to osseous tissue (McCredie, 2007). Progenitor cells that mature into osteoblasts, one of three cell types involved in bone remodeling, reside in the cambium layer (DeSaix & Johnson, 2013). The cambium is highly vascularized, systemically receiving as much as 15% of total blood volume depending on age and activity level (Karner & Long, 2018). The mineral regions of compact bone are arranged in a series of parallel, vascularized cylinders known as osteons and the blood vessels which occupy them continue through the spongy inner bone and into the medullary cavity where the bone marrow resides. In this way, all regions of the bone are in close contact with the circulatory system.

The skeleton supports an ever-changing complex of soft tissues and so itself must adapt to new conditions: micro- and macro-damage is repaired, bone mass is added to support increased skeletal muscle capability, and bone mass is lost as ions are liberated to support different physiological processes. While long-term bone mass changes are well studied, much less is known about the mechanism behind these changes. Bone remodeling is intimately tied to

exercise, as repetitive medium-intensity strain is the primary means of accruing bone mass (Han et al., 2018). Bone remodeling is also age dependent, with a general loss of both mass and density occurring with age after maturity (Fohtung et al., 2017). A reduction in inorganic bone mass corresponds with a similar reduction in the available space for osteocytes and other bone cells. Osteocytes are the most common type of bone cell and the cells which sense mechanical load on the bone, coordinating the activity of osteoblasts and osteoclasts. (Han et al., 2018, Jilka & O'Brien, 2016). The role of osteoblasts is building up bony tissue. The function of osteoblasts is opposed by osteoclasts, which resorb bone. Osteocytes develop from osteoblasts when those cells finish surrounding themselves with bony tissue, creating a niche in the bone called a lacuna where they mature into osteocytes. The lacunae are fluid filled. Osteocytes extend cellular processes out of their individual lacunae through channels called canaliculi and, in this way, form an intercellular network via gap junctions for the exchange of signaling molecules, nutrients, and waste (Busse et al., 2010, Buenzil & Sims, 2015). Through this network, osteocytes are able to send and receive signals over long distances, processing and responding to organ-scale input.

1.2 Bone Loading and Mechanotransduction

Osteocytes sense bone strain through various forms of mechanotransduction (Buenzil & Sims, 2015). Because the lacunae in which osteocytes exist are fluid filled, compression of local bone leads to fluid flow out of the lacunae. This compression impacts the membrane of the cell body and its processes. Osteocytes are able to sense the direction of fluid flow because of the directionality of the processes they have extended through the canaliculi. Models suggest that, generally, osteocytes experience between 0.8 and 3 Pa of fluid flow sheer stress due to

mechanical loading (Buenzil & Sims, 2015). The experience of an individual cell is complicated by its heterogeneous deformation (the body deforms more than the processes) and by the unique architecture of the surrounding local matrix. There is evidence that suggests much greater stress is experienced by the processes due to strain concentration in those structures. The total strain on long bones in normal human and animal locomotion is typically 0.04-0.3% of total longitudinal length during normal activity and does not exceed 1% of long bone length without severe injury (Qi & Liu, 2016).

In response to deformation of the osteocyte membrane, ion channel conductance is affected (Qi & Liu, 2016). Some types of channels implicated in the mechanosensing of bone strain include gadolinium-sensitive cation channels, L-type voltage-dependent channels, and at least three strain-responsive subunits of epithelium sodium channels. However, the distribution of these channels is not homogeneous in all long bones.

Integrins are also important in the mechanosensing of bone strain by osteocytes (Vaughan et al., 2015). It has been demonstrated that the conditional knockout of Beta-1 integrin in osteocytes led to mice which did not experience a reduction in cortical bone size with disuse of the hindlimb (Phillips et al., 2008). Additionally, it has been shown in the MLOY4 osteocyte-like cell line that degradation of the integrins which link the osteocyte process cytoskeleton to the walls of the canaliculi reduces the responsiveness of the cell to fluid flow sheer stress (Xu et al., 2012). Conversely, increased fluid flow sheer stress has been shown to increase the formation of these linkage types between the cell and the canalicular walls.

There is also a role for primary cilia in mechanosensing. Inactivation of PC1, the gene which encodes part of the primary cilia mechanosensory complex, has been shown to delay

ossification in mice while its constitutive expression lead to an increase in markers for osteoblasts (Wang et al., 2014). These data imply a role for osteocyte cilia in sensing strain.

The Mechanostat Model described local regions of bone responding to loading events in units of microstrain (fractions of the length of bone under strain compared to the same bone unstrained) (39). The equation for microstrain is:

$$\text{Strain } E \text{ at length } l \text{ and change of length } \Delta l\text{: } E = \frac{\Delta l}{l}$$

Therefore, the microstrain to which bone is subjected is dependent on the highly specific geometry of the local bone, body position, and angle of the applied force. Depending on the conditions the bone experiences, there are four tiers of strain in the Mechanostat model, each pertaining to the response the strain induces in bone (Frost 1987).

Importantly, Table 1, which shows the effects of different levels of microstrain on bone, is a generality and different bones have different thresholds for remodeling. The bones of the skull are not subjected to the same load as the tibia but nevertheless maintain their own homeostasis. For this study it is critical to understand how bones are strained and the response of bone to strain as we are using bone loading to stimulate cardiac changes.

Table 1. Generalized classes of bone strain and the effect on bone mass.

Disuse	<800 microstrain	Bone mass reduction
Adaptive State	800-1500 microstrain	Bone mass unchanged
Overload	>1500 microstrain	Bone mass increase
Fracture	>15000 microstrain	Bone fracture

1.3 Bone Remodeling

Bone remodeling occurs throughout the entire lifetime of an organism and is divided into two sub-processes: resorption and ossification (DeSaix & Johnson, 2013). Resorption is the physiological removal of bone tissue, while ossification is the physiological formation of new bone tissue. The body performs these processes to adjust to new physical demands like exercise, repair skeletal damage, and maintain homeostatic concentration of minerals stored in bone tissue. Bone adaption to exercise is especially prevalent in the femur and tibia, which are subjected to the majority of daily exercise loading through walking, running, jumping (Qi & Liu, 2016).

Mouse models deficient in osteocyte activity were shown by Tatsumi et al. to experience increased bone resorption during loading and to be resistant to disuse-driven bone loss when unloaded (Tatsumi et al., 2007). One of the major means by which osteocytes regulate resorption is by synthesizing and secreting sclerostin (Carpenter & Ross, 2020). Sclerostin acts as a paracrine inhibitor of osteoblasts via LRP5/LRP6 and inhibition of Wnt signaling (Robling & Bonewald 2020). Sclerostin also antagonizes bone morphogenic protein (BMP), which is pro-bone and -cartilage formation (St John et al., 2016). Neutralization of sclerostin with antibodies lead to an increase in the rate of bone healing after fracture (Gamie et al., 2012). The production of sclerostin is inhibited by mechanical loading (Tatsumi et al., 2007).

Another means that osteocytes use to regulate bone resorption is the production of large amounts of TGF-beta which inhibits osteoclasts activity and differentiation (Han et al., 2018). The percentage of dead osteocytes increases from less than 1% at birth to 75% by age 80 and the consequent reduction in TGF-beta leads to increased production of RANKL and M-CSF, factors

which are also secreted by osteocytes and simulate osteoclasts and bone resorption (Buenzli & Sims, 2015).

Osteocytes, sclerostin levels, and the process of bone resorption are responsive to both mechanical strain and serum ion levels (Kouvelioti et al., 2019). This is due to the skeleton's dual role in the storage of calcium and phosphate and in mechanical support of the body. Parathyroid hormone (PTH) is released when blood serum calcium levels fall too low and leads to the resorption of bone and an increase in serum calcium (Lombardi et al., 2014). The other major component stored in bone, phosphate, is similarly shifted from the skeleton to the circulation by increasing PTH. In contrast to increasing PTH, skeletal loading has been shown to increase bone mass through the sequestering of serum calcium and other components in the skeleton. It has been demonstrated that skeletal loading increases osteocyte activity, viability, and the rate of molecule transport through the osteocyte gap junction network (Batra & Jiang, 2012). These influences lead to the release of large amounts of prostaglandin E-2 (PGE2) and ATP from osteocytes (Yan et al., 2020). This release is at least partially mediated by hemichannels and gap junctions.

Thus, bone mass is in a constant flux depending on skeletal load, serum composition, and other factors; responding to these inputs bone produces factors which have been implicated in additional paracrine and endocrine roles. Specifically how these factors may affect the heart is discussed in more detail below.

1.4 Cardiac Function and Measurement

What is still not completely understood, is the effect of bone secreted factors or bone induced reflexes on cardiac function. Optimal cardiac function is determined through an

interplay of modulated systems that includes the volume of blood the heart pumps per contraction, the rate and force with which an individual contraction occurs, and the time between sequential contractions. These cardiac function parameters are known as stroke volume, contractility, and heart rate, respectively. “Cardiac output” designates the amount of blood pumped by the heart per unit time, usually per minute, and is calculated as stroke volume times heart rate (DeSaix & Johnson, 2013). “Stroke volume” is the volume of blood pumped per beat and increases with contractility. Each contraction of the heart is subdivided into systole and diastole, the period during which the ventricle is contracting and the period of time the ventricle is relaxing, respectively. Typically, such as in a medical setting when taking blood pressure, systole and diastole refer to the action of the more powerful left ventricle, although the right ventricle functions the same way. The atria also contracts, providing a relatively small amount of pressure to finish filling the ventricle with blood just before the ventricle contracts. Internally, the heart contains auto-excitable tissue in the sinoatrial node (SA) and atrioventricular (AV) node. Pacemaker cells in the SA node, located in the right atria, initiate the heartbeat, which is then propagated by conductile fibers throughout the contractile tissue of the heart (Fig. 2). The contractile tissue is a type of muscle made up of cardiomyocytes. Because propagation is not instantaneous, the regions of the heart do not contract simultaneously. Instead, the atria contract first followed by the ventricles. This is due primarily by a delay in conduction caused by cells of the AV node. This intrinsic pacing system would set the human heart rate to an approximate, relatively stable, 60 beats-per-minute (BPM) if not influenced by additional external pacing systems. The different electrophysiology of rodents means that a *ex vivo* mouse heart will intrinsically pace between 100 and 150 bpm (Sutherland et al., 2003).

Externally, the discharge rate of the SA node and the degree of delay at the AV node can be regulated by sympathetic and parasympathetic input from the Central Nervous System (CNS) (DeSaix & Johnson, 2013). A variety of sympathetic nerves originate from the central nervous system primarily from the thoracic spinal cord (T2-T5) and serve to increase cardiac output by sensitizing the SA and AV nodes to depolarization, as well as synapsing directly with the cardiac muscle tissue to sensitize cardiomyocytes to contraction. The heart is strongly influenced by this and by plasma epinephrine levels which can sensitize cardiac muscle and the SA node, drastically increasing cardiac output. In opposition to these sympathetic effects, major parasympathetic input is provided by the vagus nerve (cranial nerve X) to the SA node and AV node, which in normal circumstances sets the resting heart rate significantly lower than the heart would self-pace.

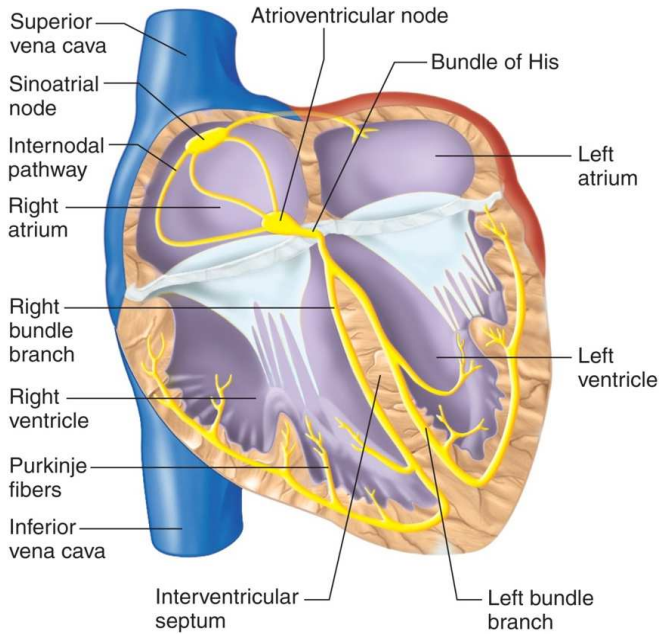

Figure 2. Anatomy of heart chambers and route of cardiac action potentials through the heart. DeSaix, P and Johnson, E. (2013). *Anatomy and Physiology*. OpenStax. https://open.umn.edu/opentextbooks/textbooks/169

Pacemaker potentials are passed to the myocardium by the Purkinje fibers (Fig. 2) (DeSaix & Johnson, 2013). When a depolarizing potential reaches a cardiomyocyte, L-type calcium channels are opened in the cell membrane and 1,4 dihydropyridine (DHP) receptors in membrane structure known as T-tubules are activated. The calcium influx through the L-type channels and the activation of the DHP receptors initiate the release of large amounts of calcium from the sarcoplasmic reticulum into the intracellular space. The combination of this calcium and extracellular calcium influx leads to the contraction of the cardiomyocyte.

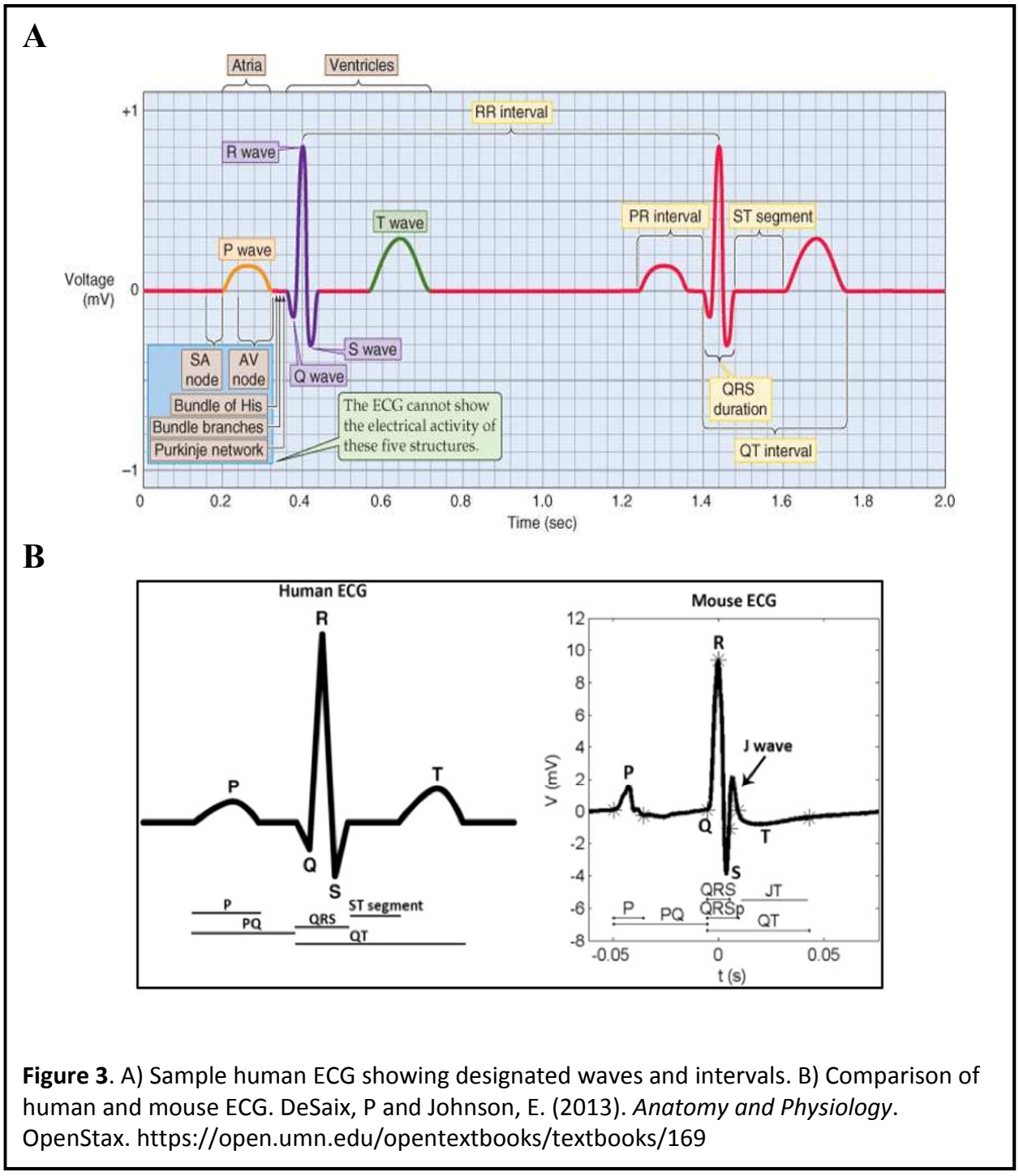

Figure 3. A) Sample human ECG showing designated waves and intervals. B) Comparison of human and mouse ECG. DeSaix, P and Johnson, E. (2013). *Anatomy and Physiology*. OpenStax. https://open.umn.edu/opentextbooks/textbooks/169

At the tissue level, the aggregate electrical currents caused by depolarizations and repolarization of regions of the hearts can be detected using sensitive techniques such as electrocardiography (ECG) (Fig. 3) (Wehrens et al., 2000). ECG is performed by placing

electrodes on the surface of the body and measuring the resistance between the electrodes over time. Each pair of electrodes is known as a lead. Three to six or more electrodes may be placed and the potential difference between each lead can be detected and recorded. Each lead produces a different "picture" of the current passing through the heart, and all of the leads can be viewed simultaneously to gain a more comprehensive understanding of cardiac behavior. These currents are recorded and processed to produce an electrocardiogram. The y-axis of an electrocardiogram represents positive and negative voltage, while the x-axis represents time. Decades of ECG data have verified the existence of established heathy patterns for each lead. Lead II is the lead typically beast able to discern all of the phases of the cardiac cycle. In Lead II, from left to right, the first positive deflection of a healthy ECG tracing, designated the P-wave, corresponds to the period of time during which the action potential is confined to the atria, after its initiation at the SA node and before it traverses the AV node. During this time, the atria contract. The following three deflections, the first one small and negative, the second very large and positive, and the third small and negative again, are known as the QRS-complex and correspond to the depolarization of the ventricle due to the pacemaker potential having traversed the AV node and spread by way of the Purkinje fibers to the myocardium at large. The final positive deflection, called the T-wave, indicates the repolarization of the ventricle. While there are some differences in the appearance of mouse and human ECGs depending on the lead used visualize them, these differences are not relevant to this study. The duration of these deflections indicates the time the heart spends completing the corresponding sub-process of each beat. The time between the deflections that together correspond to one beat and the level of synchronicity between the deflections of successive beats can communicate a great deal of information about heart function and health.

Heart rate can be determined from the time between R peaks, known as the RR interval (Wehrens et al., 2000). Variation in the time between RR peaks is known as heart rate variability (HRV) and reflects the ability of the heart to make micro-adjustments to output based on small physiological changes. A mathematical model of RR, known as SDRR, allows statistical comparison between RR intervals at different heart rates. Thus, individuals with high cardiovascular fitness present with increased HRV, while a low HRV is used as an indicator of poor prognosis following myocardial infarction (Bellenger et al., 2016). The magnitude of individual deflections within the QRS complex can indicate the degree of depolarization of parts of the ventricular myocardium while the rate at which the QRS complex and its parts occur can indicate the rate at which the action potential is able to spread. An increased QRS interval indicates the depolarization of the ventricle happens more slowly. The QT interval, the time between the initial deflection of the QRS complex and the end of the T wave deflection, reflects the time it takes for the ventricle to depolarize and repolarize. A mathematical model of QT, known as QTc, allows statistical comparison between QT intervals at different heart rates.

1.5 Bone-Heart Crosstalk; Bone as an Endocrine Organ

The endocrine role of bone is a quickly expanding field of study. Known endocrine factors derived from bone include osteocalcin, FGF23, sclerostin, PGE2, Dmp1, RANKL, PHEX, Wnt-3a, and TGF-beta. It is well established that some of these factors each play a role in muscle development, glucose metabolism, and other physiological process (Guntur & Rosen, 2012). The diverse functions of these factors are evidence of the deep interrelation between skeletal tissue and the rest of the body.

One factor which has been found to play a role in many organ systems is osteocalcin. While osteocalcin exists in a variety of forms depending on the degree of carboxylation, the two isoforms which are most common in the circulation are gamma-carboxylated osteocalcin (gla-OC) and uncarboxylated osteocalcin (glu-OC) (Moser & van der Eerden, 2019). Only the latter functions as an endocrine signal. It has been shown to be a positive driver of muscle mass via the Gprc6a receptor (Diaz-Franco et al., 2019). Strikingly, supplemental glu-OC has been shown to play a primary role in metabolic exercise capacity (Mera et al., 2016). Point-mutations which de-inhibit osteocalcin increase muscle mass. Osteocyte-specific deletion of the Cx43 gene also severely impacts muscle phenotype and the changes are partially rescued through administration of synthetic osteocalcin (Chaible et al., 2011). In vitro, osteocalcin has been shown to promote myoblast proliferation and myogenic differentiation through specific receptors (Liu et al., 2017). Osteocalcin has also been implicated in pancreas signaling, where it affects insulin secretion, in liver signaling, where is affects glucose uptake, and in signaling to adipose tissue, where it affects glucose sensitivity (Mizokami et al., 2017). Thus, osteocalcin may prove a potential target for diabetes mellitus treatment. Osteocalcin has also been shown to increase during certain types of exercise and support optimal exercise capacity of myofibrils (Hiam et al., 2019). There is a link between osteocalcin and vascular calcification, including calcification of the heart valves, but the process appears mediated by other metabolic factors (Tacey et al., 2018). A small study by Zhang et al. found a correlation between high circulating osteocalcin and decreased risk of chronic heart failure (CHF), even when controlling for other factors such as exercise level (Zhang et al., 2010). Recently, Berger et al. determined that circulating undercarboxylated osteocalcin increased 50-150% in mice following psychologically stressful stimuli, and in humans in stressful situations (Berger et al., 2019). This was accompanied by an increase in heart

rate and blood pressure without an increase in any other bone-derived factor. It was also found that this osteocalcin was released specifically from skeletal osteoblasts, and that it was sufficient, even in adrenalectomized mice, to illicit a physiological response to acute stress, including the acute changes in cardiac function. Osteocalcin has also been shown to play an important role in adapting to exercise and promoting exercise capacity, even restoring the capacity of elderly mice to that of young mice (Mera et al., 2016).

The bone-derived hormone FGF23 has also been shown to have a wide range of physiological effects. Produced by osteocytes and osteoblasts when plasma phosphate levels are high, FGF23 plays a central role via the kidneys in maintaining systemic phosphate and vitamin D levels (Richter & Faul, 2018). In addition, FGF23 knockout mice develop hypoglycemia and reduced sensitivity to insulin (Bar et al., 2018). Our group has shown that in the hypophosphatemic rickets model, *Dpm1-/-*, mice have significantly reduced skeletal muscle function (Wacker et al., 2016). The Wacker laboratory has been particularly interested in the effects of FGF23 on cardiac function. Dr. Wacker and others have shown that FGF23 can induce ventricular hypertrophy and arrhythmias (Graves et al., 2021). FGF23 is a strong predictor of cardiovascular failure in CKD patients when other factors are controlled for (Poelzl 2014). By definition, CKD is a progressive decrease in glomerular filtration rate (GFR), the leading cause of which is chronic high blood pressure. Comorbidities of CKD include pulmonary and peripheral edema, hypertension, and cardiovascular disease, symptoms which drive the progression of the root disease. As their GFR decreases, CKD patients experience increased levels of circulating FGF23 and parathyroid hormone with, in the later stages, decreasing 1,25 Dihydroxyvitamin D and increasing phosphate (Felsenfeld et al., 2015). Interestingly, the increase in FGF23 proceeds the other changes in serum composition. The increase in FGF23

seen in CKD has so far been considered a symptom dependent on falling GFR and mishandling of calcium and phosphate. However, relevant is the fact that high serum FGF23 is associated with left ventricle hypertrophy, decreased ejection fraction, arrhythmias, and heart failure, the very symptoms which drive the progression of CKD (Vogt et al., 2019). This suggests FGF23 may be a potential therapeutic target, or may even, conceivably, play a role in initiating the disease process. Clinical studies had previously associated FGF23 with increased cardiac mortality (Poelzl 2014), but Faul et al. showed that FGF23 was specifically and independently associated with left ventricular hypertrophy (LVH) in a large, diverse group of CKD patients (Faul et al., 2011). Furthermore, they showed that FGF23 activated the calcineurin-signaling pathway and lead to the hypertrophy of isolated rat cardiomyocytes and that intravenous injections of FGF23 caused LVH in otherwise healthy wild-type mice. Our lab followed this work by showing that FGF23 significantly increased the size and the expression of cardiac hypertrophy gene markers in cardiomyocytes in vitro (Touchberry et al., 2013). We also found that CKD-model mice had elevations in gene markers for cardiac hypertrophy, reduced fractional shortening, and reduced ejection fraction at just 10 weeks of age. Central to the hypothesis of this thesis, our lab's previous work also showed acute elevations of intracellular calcium when cardiomyocytes were exposed to FGF23 and a 67% increase in ventricular muscle strip contractility when the strips were exposed to FGF23. Another group was able to show using the patch-clamp method that FGF23 increased the L-type calcium channel currents and the calcium content of the sarcoplasmic reticulum in HL-1 cells (Kao et al., 2014). They also observed increased phosphorylation of calcium/calmodulin-dependent protein kinase II which was reversed by a subsequent FGF receptor inhibitor treatment.

Another bone derived factor, sclerostin, is excreted by mature osteocytes and is a known suppressor of the Wnt/beta-catenin pathway (Ellies et al., 2006). By inhibiting Wnt-3a, the differentiation of C2S12 immortalized myoblast is inhibited. A loss of function mutation in the sclerostin gene, *SOST*, leads to low sclerostin levels and a reduction in bone mass. Sclerostin has not been shown to increase during bedrest or unloading, but to decrease following bone loading, suggesting a set-point for bone mass maintenance (Delgado-Calle 2017). The administration of sclerostin antibodies has been shown to increase bone mass in mice (Gamie et al., 2012)). Sclerostin is strongly associated with increased cardiac valve calcification in patients with CKD (Ji et al., 2018) and with increased pulse wave velocity in dialysis patients (Stavrinou et al., 2019).

PGE2 has wide ranging physiological effects in the processes of inflammation, muscle healing, and the development of cancer (Mo et al., 2012). Sheer stress can release large amounts of PGE2 from osteocytes' hemichannels, increasing PI3K and activating the beta-Catenin pathway (Xia et al., 2010). PGE2 has been shown to increase survivability of osteocytes and increase bone formation, and to promote the proliferation of myoblasts (Jiang et al., 2007). PGE2 has been shown to reduce cardiac contractility via the EP3 receptor both in isolated cardiomyocytes and whole-heart models (Gu et al., 2016). At the same time, there is evidence for its involvement in cardiac repair fibrosis (Ma et al., 2018).

The myriad of evidence that bone-derived factors effect diverse organ systems, with many examples effecting the heart specifically, suggest the possibility that these factors may affect cardiac function on a daily basis. The production of many of these factors are directly affected by states of skeletal loading, a condition very often experienced during exercise conditions, such as when prey tries to avoid predators. Thus, it seems likely that bone-derived

factors may play a direct, acute role in cardiac performance and if so, this fact may help explain the observed association between many of these factors and more chronic heart pathologies.

1.6 Hypothesis

In conclusion, the skeleton appears to be in complex interaction with many organ systems, producing important factors which affect diverse bodily functions. Additional research is needed however to elucidate what effect, if any, is induced in the heart by bone strain. It would be logical from an evolutionary standpoint if exercise-induced bone strain supported the increased cardiac function necessary for that physical activity. It is the hypothesis of this research that bone strain, separate from skeletal muscle activity and environmental stress, will lead to an increase in cardiac output. Two methods were used to investigate this question. First, through the culture of MLO-Y4 osteocyte-like cells under conditions modeling the stress they would experience inside bones during exercise and qualification of affects by the administration of the conditioned media to Langendorff-perfusing murine hearts. Second, through cardiac ECG data collected on live mice in a precision loading apparatus designed to induce exercise-modeling tibia strain independent of skeletal muscle contractions or limb movement and the subsequent quantification of released factors in the blood by high pressure liquid chromatography (HPLC).

CHAPTER 2

MATERIALS AND METHODS

2.1 MLO-Y4 Cell Fluid Flow Sheer Stress-Conditioned Media

Conditioned media was prepared from MLOY-4 osteocyte-like cells. On day 1, MLO-Y4 cells were seeded onto collagen-coated positive-charged slides at a cell density of 5,600 cells/cm^2 on six slides with an area of 18.75cm^2 per slide for a total 6.3 X 10^5 cells. After an initial 2-hour incubation in 2.5% calf serum (CS) and 2.5% fetal bovine serum (FBS) containing alpha-MEM containing 1% penicillin/streptomycin to allow proper adherence to the plates, the cells were covered in an additional 15 mL of this media. On day 2, sheer stress of 2 dynes/cm^2 was applied to 6 slides for 2 hours in 350 mL of 2.5% CS and 2.5% FBS containing alpha-MEM (1% P/S). The media was collected from the six slides after 1 hour of shear stress and combined. Approximately 300 mL of conditioned media was collected for experimental use, aliquoted, and stored at -20 C. 2.5% CS and 2.5% FBS containing alpha-MEM (1% P/S) not used for culturing cells was used as the vehicle control.

2.2 Externally-Paced Heart Langendorff Procedure

Sixteen-week-old male CD1 mice were anesthetized using 3% isoflurane. Their chest cavities were opened and hearts excised. Hearts were transferred to a petri dish containing 3 mL of Ringer's perfusion buffer (NaCl 140 mM, CaCl2 2.5 mM, KCl 2.0 mM, K2HPO4 1.5 mM, MgSO4 1 mM, HEPES 10 mM, glucose 10 mM, and pH 7.4). The atria and SA node were quickly removed. A flexible cannula was inserted and tied into the aorta through which the hearts were perfused with oxygenated Ringer's solution at a rate of 1.2 mL per minute. The

Langendorff-perfused hearts were then attached to a force transducer via suture and suspended in a bath of circulating ringer's buffer (see Fig. 4). The hearts were suspended between electrodes to electrically pace the heart. Because the SA nodes were removed, heart rate was stimulated at 2.0 Hz/ 1.6 V/ 4 mS duration (Grass SD900, Sequim, WA). The hearts were allowed to stabilize for 15 minutes. The contractile parameters of the perfused hearts were tested using five different concentrations of MLO-Y4 conditioned media or unconditioned media (vehicle). The concentrations tested were 7.5x10^-4%, 7.5x10^-3%, 7.5x10^-2%, 7.5x10^-1%, and 7.5% (percentages were determined as the concentration of media in the total volume of the Ringer's heart solution in the closed-loop Langendorff system). One set of hearts was tested using the three higher concentrations, beginning with 7.5x10^-2% and ending with 7.5% (n=6), while a different set of hearts were tested at the two lower concentrations (n=3). Contractile force was monitored and recorded via LabChart software (ADInstruments, Colorado Springs, CO). The two minutes immediately prior to the addition of media or vehicle established the baseline contraction parameters. After the addition of media or vehicle, data was collected for 30 minutes. Reported contraction values were determined by averaging the area of greatest change (averaged over two minutes) starting 30 seconds after the addition of media or vehicle. Determining the number of premature beats (arrhythmias) was accomplished using LabChart software to identify the number of observed contractions over the 30-minute period after the addition of media or vehicle and comparing that to the number of contractions expected based on the external electrical pacing rate of the heart.

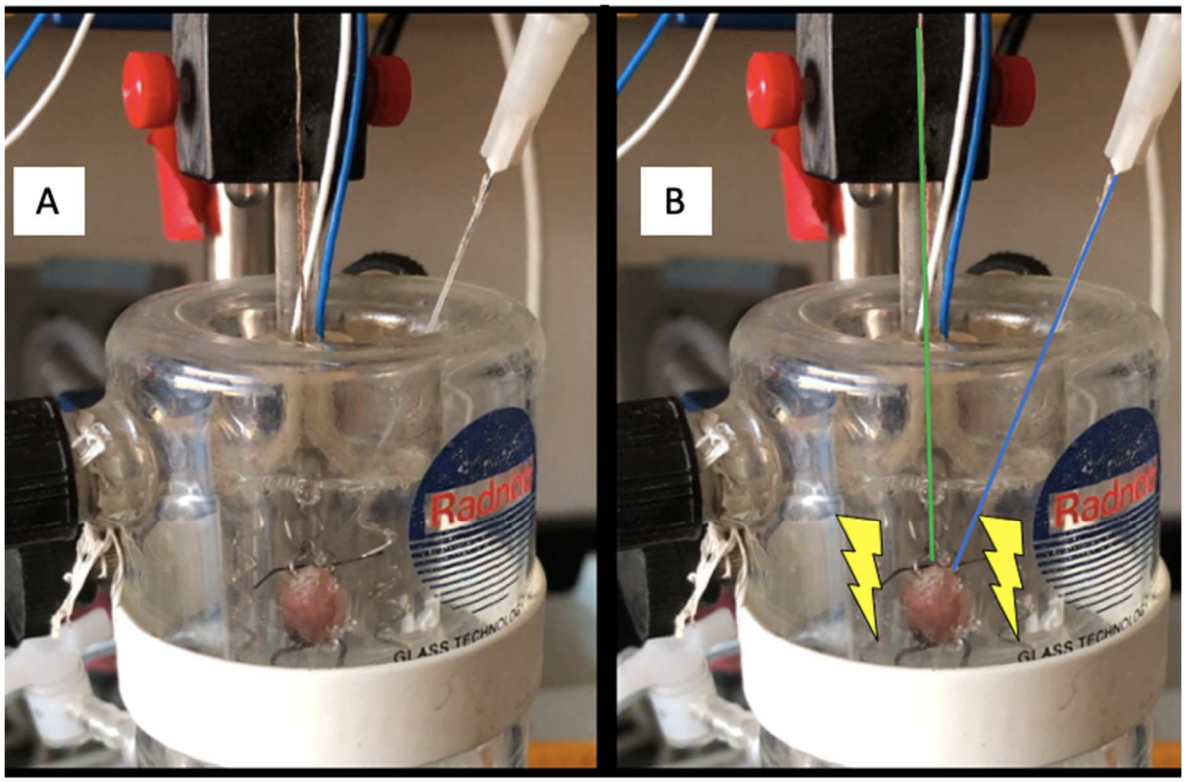

Figure 4: Perfused heart contractility experimental setup in oxygenated Ringer's bath. (A) Langendorff-perfused heart with external pacing electrodes and force transducer. (B) Same image, with yellow bolts highlighting the location of the pacing electrodes, blue line highlighting the cannula delivering Ringers solution to the aorta, and the green line highlighting the connection of the heart to the force transducer.

2.3 Self-Paced Heart Langendorff Procedure

To determine if the contractile responses would be different using a different pacing rate, hearts were testing using their intrinsic sinus rhythm. This procedure differed from the externally-paced Langendorff procedure only in that the atria and SA node were not removed and external electrodes were not used to pace the heart. Vehicle and conditioned media were testing in the same manner as above.

2.4 Two-Minute Tibia Strain and EKG Procedure

Six-month-old CD-1 mice were anesthetized and maintained on 3.0 % isoflurane and secured in a precision bone loading apparatus (see approved IACUC Protocol: Wacker-2001). The right rear leg of the mouse was positioned for loading by placing the heel of the foot in a divot and the knee in the loading cup of the loading apparatus (See Fig. 5). Twenty-nine-gauge needle EKG leads were inserted into the skin and a rectal temperature probe was inserted. Body temperature was monitored and maintained between 36.0-37.0 C° using a circulating water heating pad. Loading occurred without flexion of the knee or ankle joint or significant shortening of any of the large limb muscles. The tibia, via the knee and heel, was cyclically loaded with 9N of force at a frequency of 2 Hz for 120 seconds. An ECG baseline was established before loading began and data were collected throughout the loading process and during a 30-minute period after loading. Heart rate, QRS, QTc, and SDRR were measured. Data points were averaged over

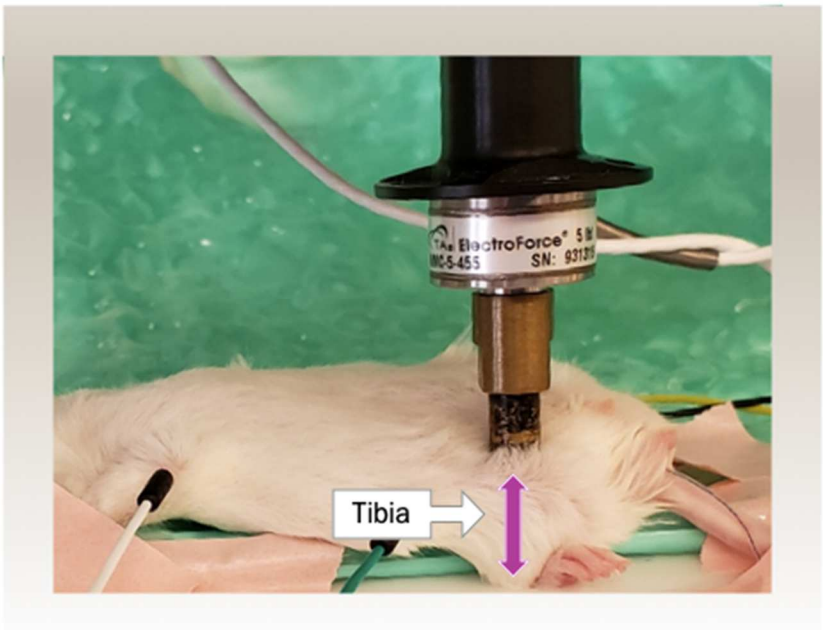

Figure 5: Sample loading procedure with an anesthetized mouse showing loading apparatus placement around the tibia, ECG lead placement, and temperature probe placement. Water jacketed heating pad (green) was placed underneath the mouse to maintain body temperature.

two minutes. After the end of the experiment a blood sample was taken via cardiac puncture and a second method of euthanasia was carried out using cervical dislocation. Blood samples were maintained at -80° C until processing.

2.5 Blood Sample Extraction for Liquid Chromatography/Quadrupole Time of Flight Mass Spectrometry (LC/QToF MS)

Blood samples were used to analyze metabolite profiles after loading. The first extraction solvent was made using 80% methanol with 10 μM Umbelliferon as internal standard. Five hundred μL of the first extraction solvent was added to 100 μL of the serum samples. The resulting mixture was kept on ice for 15 minutes with intermittent shaking. Centrifugation at 6000g and 4 °C for 20 minutes was then used to pellet the cell debris and the first supernatant was collected. A second extraction solvent was then made using 67% methanol/water without any internal standards added. The cell debris pellet was resuspended in this second extraction solvent by vortexing and pipetting. Centrifugation at 6000g and 4 °C for 20 minutes was again used to pellet the cell debris and the supernatant was collected a second time. This second supernatant extract was then combined with the first supernatant extract. Two-hundred fifty uL of HPLC-grade water was added to the combined extract, mixed well, and then the mixture was frozen at -80 °C. The frozen sample was dried at high vacuum (<50 um Hg). The dried samples were next dissolved in 200 μL of 3.5% acetonitrile/96.5% water and stored at -20°C prior to analysis. Intracellular metabolites from each biological replicate were extracted using a cold methanol extraction. Two hundred and fifty microliter methanol was added to the cell pellet and the samples were mixed vigorously for ~1 min on a vortex machine, then 50 ul isotope-labelled amino acid mixture was added as internal standards (Cambridge Isotope Laboratories, Tewksbury, MA, USA) and then mixed one more

time. The mixture was stored at 20°C for 20 min and centrifuged for 20 min. Then 150 ul of the supernatant was collected and dried on a vacuum concentrator. The dried sample was later reconstituted by 50% H2O and 50% acetonitrile and kept in 4°C auto sampler for MS runs.

2.6 LC/QToF MS Analysis Settings and Gradient

A Thermo Scientific Ultimate 3000 HPLC coupled with a TSQ Quantiva Triple Quadrupole mass spectrometer was used in this study. A hydrophilic interaction chromatography (HILIC) column was purchased from Waters Corporation (Milford, MA, USA). The chromatography method operated as previously described (3010). Briefly, analytical grade standard chemical compounds corresponding to the measured metabolites were purchased from Sigma-Aldrich (Saint Louis, MO, USA) or IROA Technologies (Boston, MA, USA). LC– MS-grade acetonitrile, ammonium acetate and acetic acid were all purchased from Fisher Scientific. We used flow rate of 0.300 ml min1 for HPLC separation, with autosampler temperature kept at 4°C, and the column compartment set at 40°C. The total separation for both positive and negative ionization modes was 20 min. The mobile phase was composed of 5 mM ammonium acetate in 90% H2O/10% acetonitrile + 0.2% acetic acid as solvent A and 5 mM ammonium acetate in 10% H2O/ 90% acetonitrile + 0.2% acetic acid as solvent B. The gradient separation lasts for 11 min and then the column was washed for additional 9 min to avoid potential carry- over. The targeted metabolic profiling was performed in selected-reaction-monitoring (SRM) mode, established by running multiple standards first, and then using the obtained retention time and SRM transition information to search for the presence of targeted metabolites from unknown samples. Pooled quality control (QC) samples were also run between every ten samples to ensure the performance of the method.

2.7 Statistical Analysis of Liquid Chromatography/Quadrupole Time of Flight Mass Spectrometry (LC/QToF MS) Results

All raw data were manually inspected using the Quan browser module of XCALIBUR version 4.0 (Thermo Fisher Scientific). Then the data were filtered using the threshold of 80% (meaning the metabolite must be detectable in 80% of the samples from the same group). Data were then processed through log transfer and autoscaling to achieve normal distribution. The reproducibility of our method was defined by the average coefficient of variation value (average CV), which was calculated using standard deviation of each metabolite from all the QC samples divided by their average (defined as coefficient of variation), and then this value is added together and again divided by number of metabolites detected. Both univariate (ANOVA) and multivariate (principal components analysis) statistical analyses were applied using JMP PRO12 (SAS Institute, Cary, NC, USA) and SPSS Version 22.0 (IBM Corp. Armonk, NY, USA). These two methods were selected because they were commonly applied in metabolomics field in understanding both individual metabolite significance and the overall metabolic significant that is mostly suitable by multivariate data analysis. Full data set were used for all the principal component analysis. Metabolic pathway analysis was performed using the online tool METABOANALYST 3.0.

CHAPTER 3

RESULTS

3.1 Effects of Bone Conditioned Media on Isolated Heart Contractility

To determine if bone conditioned media altered ventricular muscle contractility in the setting of artificial electrical pacing, we used isolated, Langendorff-perfused hearts lacking atria and paced at 2 Hz. Contraction waveforms of the Langendorff-perfused hearts in the presence of bone conditioned media or vehicle were recorded as force vs time (Fig 6A). From these

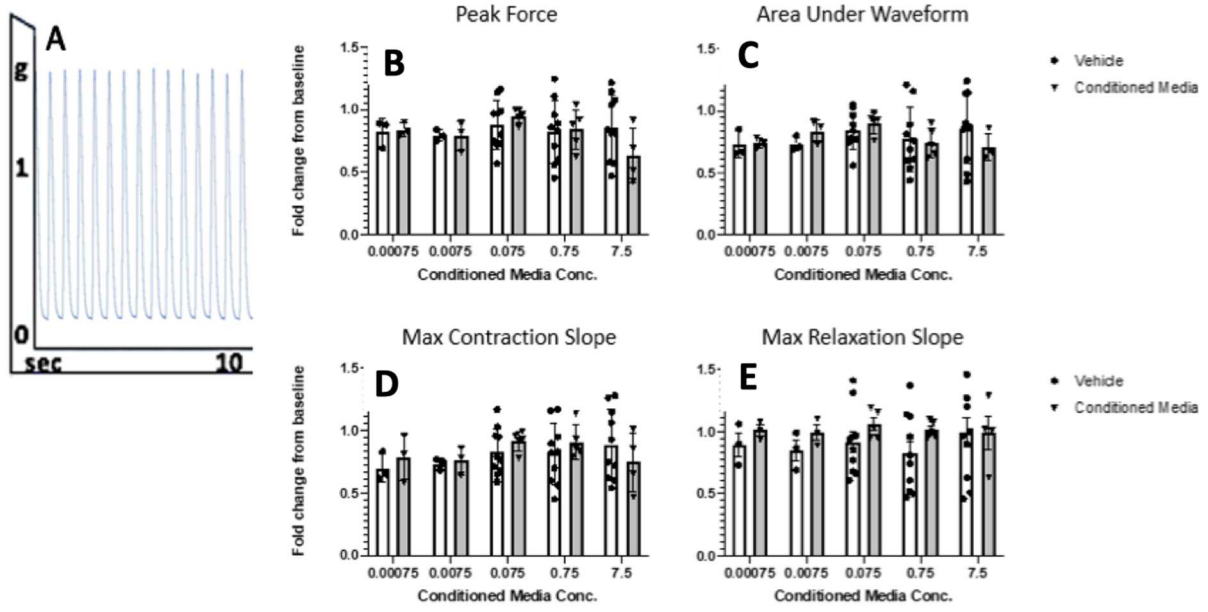

Figure 6: Bone Conditioned media effects on paced hearts. Cardiac muscle contractile waveform analysis was conducted after five concentrations of media (0.00075%, 0.0075%, 0.075%, 0.75%, and 7.5%) were tested against equal volumes of vehicle on 16-week-old male CD-1 mouse hearts by perfusion through the Langendorff apparatus paced at 2 Hz. Changes were normalized to baseline readings collected before the addition of vehicle or bone conditioned media. A) Example of raw heart contractility force tracing. B) Average maximum peak rate of contraction force. C) Average total area under individual contractile waveforms. D) Average rate of contraction. E) Average rate of relaxation. Two-way ANOVA with post-hoc Tukey was performed ($P>0.05$; n= 3-10).

records we quantified the maximal contractile force, the rate of force production, the rate of relaxation, and the total force (area under waveform) produced by the heart. Average peak force values (Fig 6B), total force produced (total area under the waveform; Fig 6C), maximal contraction rate (Fig. 6D) and relaxation rate (Fig. 6E) were not statistically significantly different compared to vehicle in any of the concentrations of bone conditioned media tested ($P>0.05$; $n=6$).

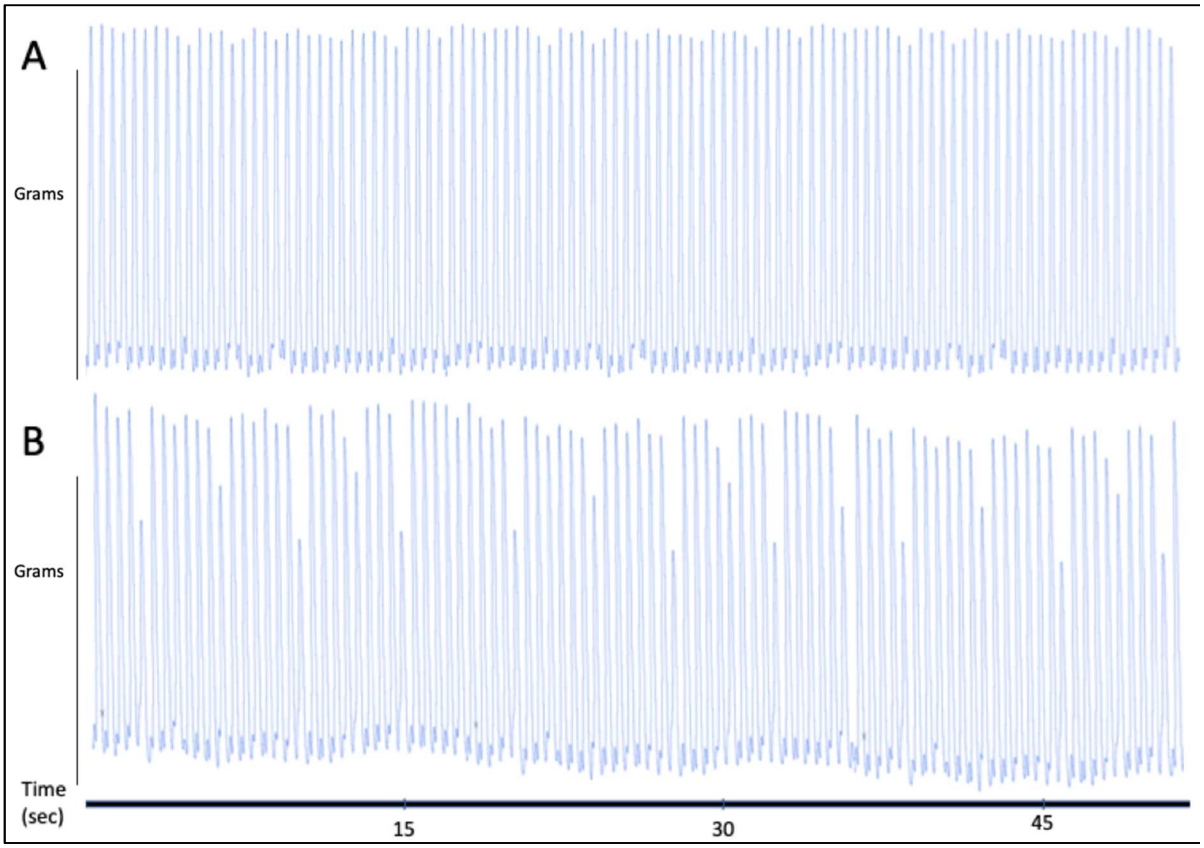

Figure 7: Sample Langendorff-perfused heart contractility waveforms of hearts paced at 2 Hz. A) Typical contraction waveform pattern of control hearts. B) Typical contraction waveform pattern of hearts treated with 7.5% bone conditioned media showing premature and abnormally shaped contraction peaks.

Interestingly, although the contractility parameters were not statistically different after treatment with bone conditioned media, we observed persistent early contraction peaks out of rhythm with the electrical pacing rate and of abnormal magnitude compared to controls (premature ventricular contractions) (Fig 7). The premature contractions observed after the application of bone conditioned media or control were quantified. Figure 8A shows the rate of premature contractions. Addition of vehicle to the heart contractility chamber resulted in an increase in the rate of premature contractions to approximately 1.5/min. However, when bone

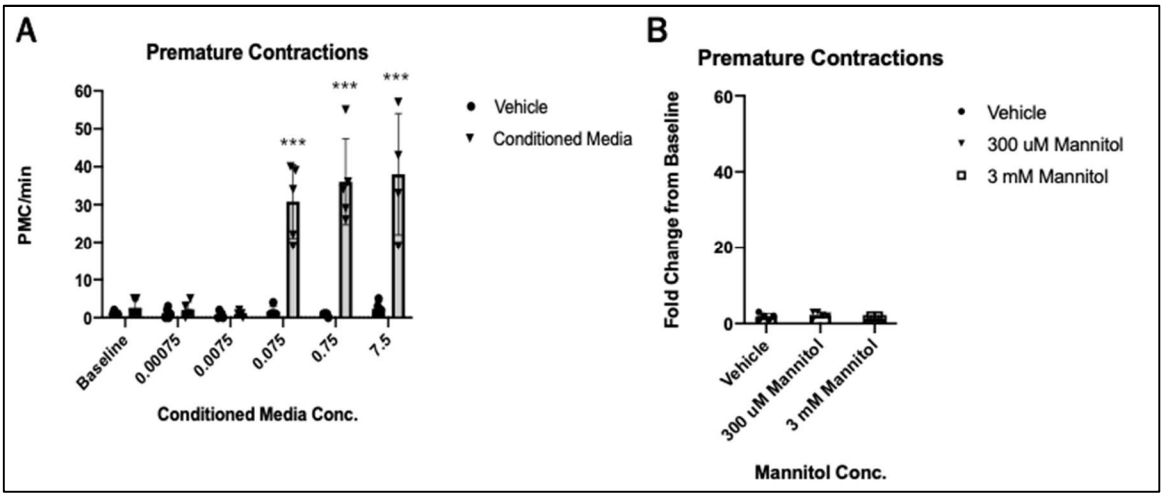

Figure 8: Bone conditioned media effects on premature contractions. Changes in number of premature ventricular contractions were analyzed after using five concentrations of bone conditioned media (0.00075%, 0.0075%, 0.075%, 0.75%, and 7.5%). Contraction changes were tested on hearts excised from 16-week-old male CD-1 mice by perfusion through the Langendorff apparatus. Changes were normalized to baseline readings collected before the addition of vehicle or bone conditioned media. A) Rate of premature contractions 5 min before and 5 min after adding bone conditioned media. (***P<0.001 compared to vehicle; n=5) Two-way ANOVA with post-hoc Tukey. B) Mannitol was used to alter the molarity of the heart bath during pacing as a control test. Two concentrations (300 uM and 3 mM) were tested. (n=5, P<0.05).

conditioned media was added the premature contraction rate increased to over 30/min at the concentrations of 0.075%, 0.75% and 7.5% ($P<0.001$). Lower concentrations of 0.00075% and 0.0075% bone conditioned media did not elicit these changes to premature contraction rate. To ensure that the observed changes in muscle contractile rhythms were not due to changes in osmolarity caused by adding a higher percentage of bone conditioned media, a series of experiments was repeated using mannitol to increase osmolarity. Figure 8B shows that using mannitol to increase the osmolarity of the heart bath by 300 uM and 3 mM did not increase the rate of premature contractions compared to vehicle ($P>0.05$).

3.2 Isolated Heart Contractility Measurements in Self-Paced Hearts

Experiments were repeated using Langendorff-perfused hearts with intact atria and SA nodes, allowing hearts to pace themselves spontaneously during the experiments without electrical stimulation. Contraction parameters of the Langendorff-perfused hearts were analyzed before and after administration of bone conditioned media (Fig 9). The addition of 0.075% and 0.75% bone conditioned media did not induce the acute changes in heart rhythm seen in externally paced hearts (Fig 9A). As such, premature contraction rate (Fig 9B) was found to be not significantly different than vehicle. Interestingly, bone conditioned media did not alter heart rate (Fig 9C). However, both total force (area under the waveform) (Fig 9D) and peak force generation (Fig 9E) were increased significantly after bone conditioned media was added, compared to vehicle ($P<0.001$-0.01). The rates of contraction (Fig 9F) and relaxation (Fig 9G) were not significantly altered by bone conditioned media when the heart was able to self-pace.

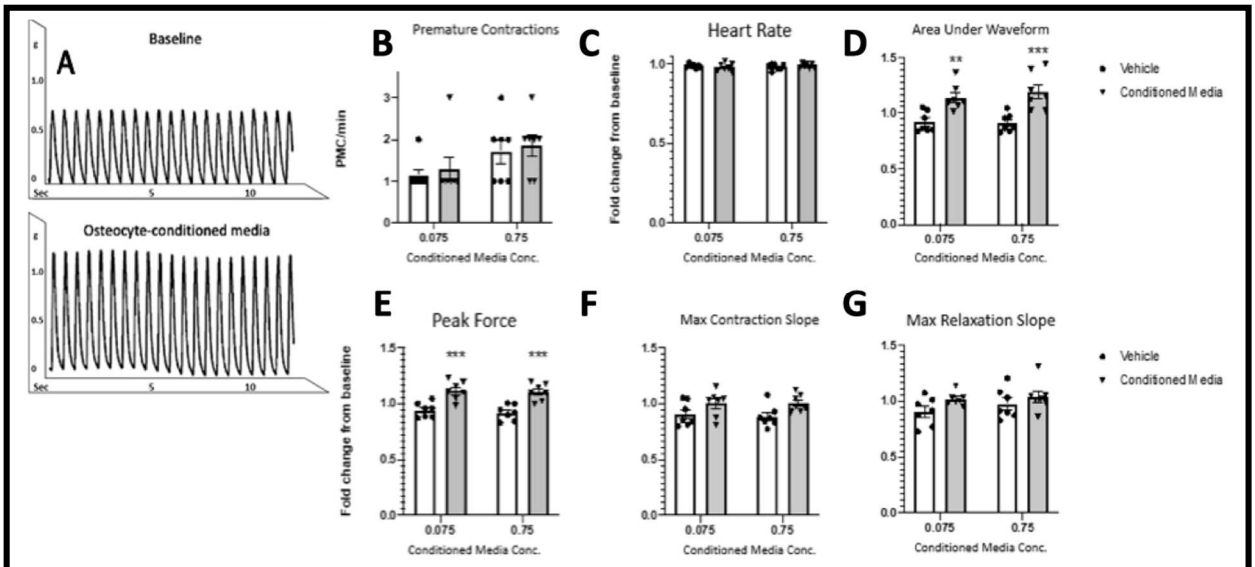

Figure 9: Bone conditioned media effects on self-paced hearts. Two concentrations of media (0.075% and 0.75%) were tested against equal volumes of vehicle on 16-week-old male CD-1 mouse hearts by perfusion through the Langendorff apparatus while allowed to self-pace. Changes were normalized to baseline readings collected before the addition of vehicle or bone conditioned media. A) Example whole heart contractile force tracing before and after bone conditioned media was added. B) Rate of premature contractions before and after bone conditioned media was added. C) Average heart rate of self-paced hearts before and after bone conditioned media was added. D) Average total area under individual contractile waveforms (total force produced during a contraction). E) Average peak force of contraction. F) Average rate of contraction. G) Average rate of relaxation. (** P<0.01, ***P<0.001 compared to vehicle; n=6-7).

3.3 ECG Measurements During *in vivo* Bone Loading

Figure 10 is based on ECG readings we took of whole-animal models subjected to compressive tibia loading in a precision loading apparatus. ECGs were collected before, during, and after 2 minutes of tibia loading. A distinct reduction in heart rate of as much as 50 bpm was noted by ECG as soon as tibia loading began (Fig 10A). The majority of this reduction proved temporary and a nearly complete recovery of heart rate to baseline levels was observed in all

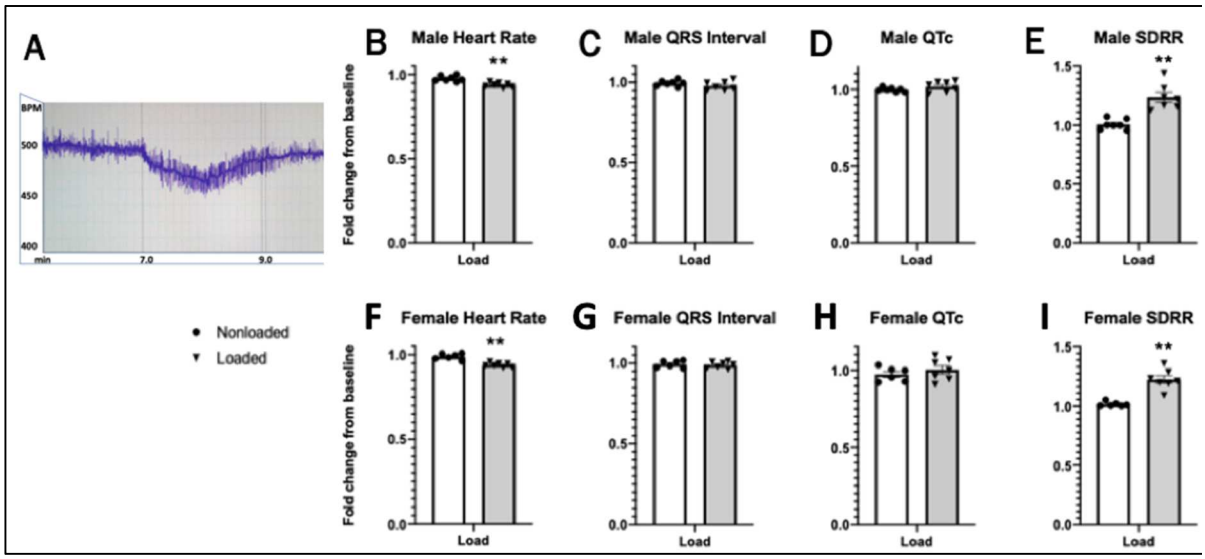

Figure 10: Two-minute tibia loading effects on ECG. ECG data was collected during *in vivo* tibia loading and during simulated loading in the loading apparatus (non-loaded control). Changes were normalized to baseline readings collected before tibia load. A) Example heart rate tracing immediately before, during, and after tibia load. B, F) Average heart rate of males and females. C, G) Average QRS intervals. D, H) Average QTc interval. E, I) Average SDRR (heart rate variability). (** P<0.01 compared to vehicle; n=6-7 for both male and female mice).

animals of both sexes by the end of the 2-minute loading period. This reduction in heart rate was statistically significant during the two minutes of loading (Fig 10B, F) compared to control as measured as a change in baseline established using the average of the two minutes immediately prior to the start of loading (P<0.01). No statistical change was observed in the ECG waveform parameters QRS (Fig 10C, G) or corrected QT interval (QTC) in either sex (Fig 10D, H). A significant increase in heart rate variability during the loading period, as indicated by SDRR, was also observed in both sexes (P<0.01) (Fig 10E, I).

3.4 Measurement of Post-Loading Blood Metabolites by Liquid Chromatography/Quadrapole Time of Flight Mass Spectrometry (LC/QToF MS) Analysis

Finally, we wanted to assess differences in the blood metabolite profiles of tibia-loaded and control mice, which could indicate potential paracrine or endocrine factors altered by bone loading and serve as indications of potential bone-heart crosstalk mechanisms. Following the experiments in which tibia loading was conducted, ECG monitoring continued for 28 minutes after loading ended and then a blood sample was collected. Analysis of the samples using LC/QToF MS identified the metabolites of the samples.

Figure 11 shows the univariate analysis and resulting Volcano Plots when the serum metabolites of 2-minute loaded and control males (11A), 2-minute loaded and control females (11B), and all 2-minute loaded and controls (11C) are compared. These volcano plots compare the degree to which the concentration of a serum metabolite was increased (red dots) or decreased (blue dots) to the probability that the change was not statistically random (y-axis). When multivariate statistical analysis using principal component analysis followed by partial-least squares discriminate analysis was performed, we detected six significantly altered metabolites in the blood of loaded male mice and five in loaded female mice. When the altered metabolites of both male and female groups were combined, the concentration of one particular metabolite, (acetic acid--heptadeca-1,9,16-triene-4,6-diyn-3-ol) was found to be significantly elevated. This metabolite is highlighted in Table 3, which lists all of the metabolites from both males and females which were statistically altered. No other metabolite, besides the highlighted one, was altered in both male and female 2-minute loading groups.

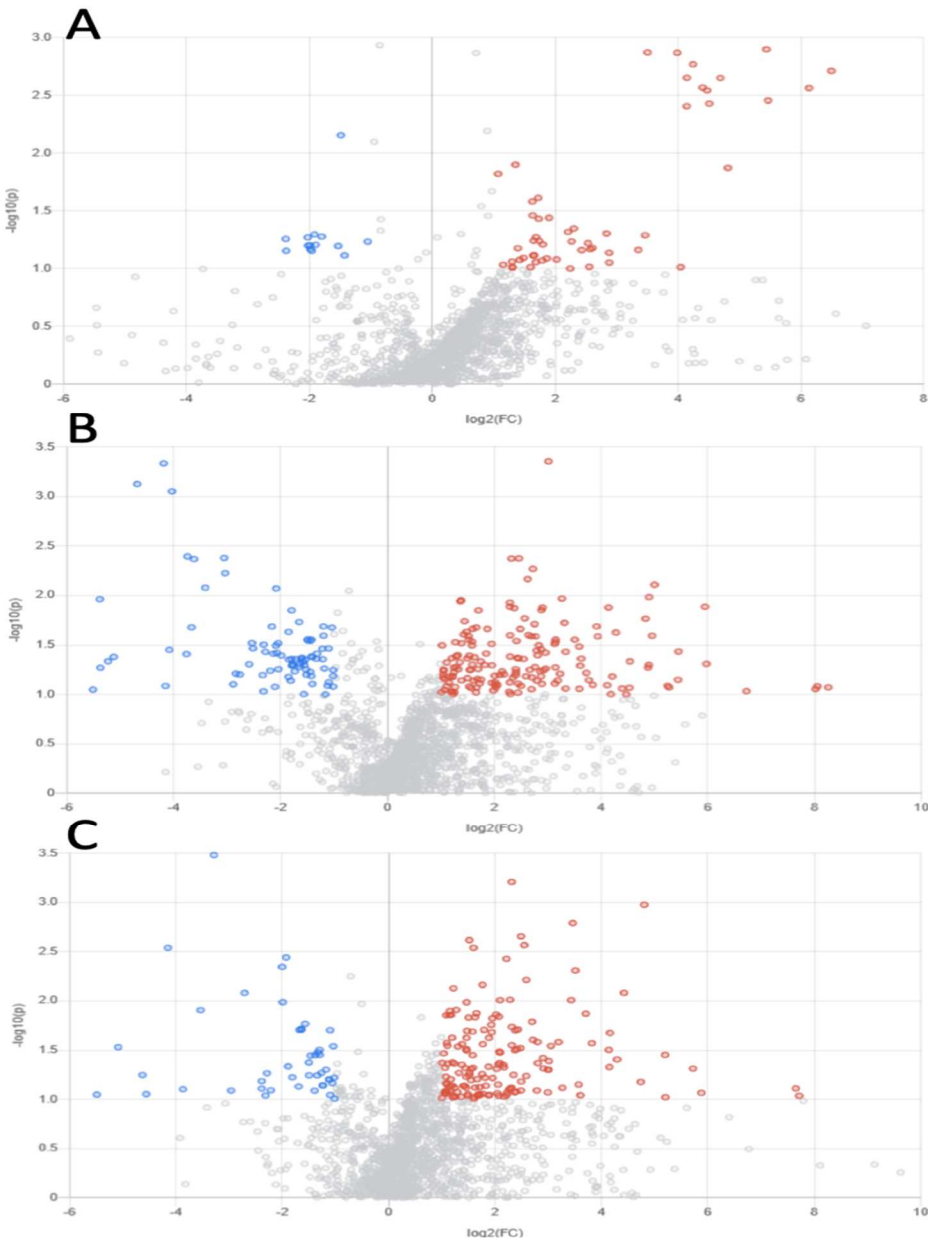

Figure 11: Significant increases/decreases in metabolites after tibia load. Volcano plots generated by analysis of serum samples for lipid metabolites using LC/QToF MS. Statistically significant increases in metabolites are indicated by red dots while decreases are indicated by blue dots. A) Volcano plot comparing 2-min loaded males with 2-min male controls. B) Volcano plot comparing 2-min loaded females with 2-min female controls. C) Volcano plot comparing all 2-min loaded with all 2-min controls. Plots represent the relationship between the log of fold change (x-axis) and probability as calculated by T-test (y-axis).

Table 2: Mass of LC-QToF-MS-Derivatized Metabolites of Significance and Their Presumptive Chemical Identities

Mass	Retention Time	Sex	Presumptive Identity
258.2	18.8	Male	1,3-Dimethyl-N,N-bis(trimethylsilyl)-1,3,2-diazaborolidin-2-amine
272.2	19.2	Male	1-(4-Phenoxyhept-2-yn-1-yl)piperidine
278.0	21.6	Female	(2Z)-{2-[(Chloroacetyl)amino]-1,3-thiazol-4-yl}(methoxyimino)acetic acid
278.9	0.8	Male	1,3,4,6-Tetrachloroglycoluri
303.2	**22.3**	**Male & Female**	**Acetic acid--heptadeca-1,9,16-triene-4,6-diyn-3-ol**
399.3	22.4	Male	6-(hexadecylamino) quinoline-5,8-dione
524.4	21.7	Female	3-(Diphenylphosphanyl)-N-methyl-N-octadecylpropanamide
599.6	14.0	Female	N,N-Didodecyl-N-methyldodecan-1-aminium nitrate
898.9	14.0	Female	Difluoro[tris(undecafluoropentyl)]-lambda~5~-phosphane
899.4	14.1	Male	4-Methoxyphenyl 2,3,6-tri-O-benzyl-4-O-(2,6-di-O-benzyl-beta-D-galactopyranosyl)-beta-D-glucopyranoside

Lastly, Figure 12 shows clustering of the most significant serum samples based on their components using a 2D orthogonal partial least-squares score plot. Loaded females (12B) showed more distinct clustering and separation compared to controls than did loaded males (12A). Groupings persisted when the male and female data was combined (12C).

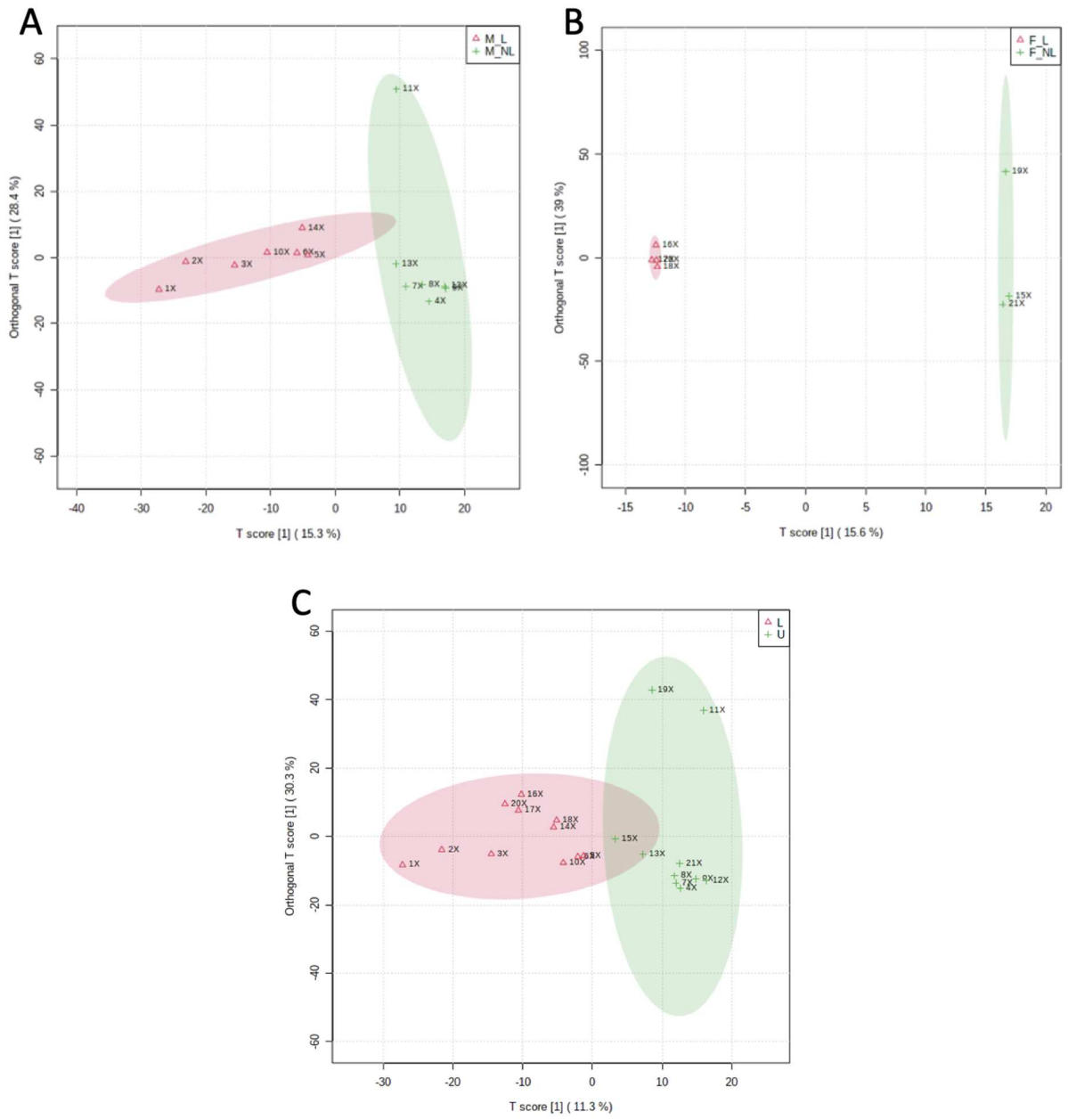

Figure 12: Principal component analysis (PCA) score plot comparing metabolic profiles of loaded vs unloaded groups. (A) Score plot comparing 2-min loaded (red) with 2-min control (green) males. (B) Score plot comparing 2-min loaded with 2-min control females. (C) Score plot comparing all 2-min loaded with all 2-min controls. The shaded area indicated the 95% confidence region.

CHAPTER 4

DISCUSSION

4.1 Introduction to Discussion

The skeleton is a dynamic organ system in constant communication with other parts of the body. Factors produced in bone go on to have significate effects on other organ systems such as the gut, kidney, brain, and skeletal muscle. Our groups and others have demonstrated that specific factors released by bone, such as FGF23, directly impact the heart (Touchberry et al., 2013, Graves et al., 2021). These effects include changes in intracellular calcium, cardiac contractility and cardiac remodeling. Here, we investigated if media collected from cultured bone cells under shear stress as well as acute loading of bone alter cardiac function which would provide further understanding of bone-heart crosstalk. We did this first by measuring contractility and heart rate changes in *ex vivo* murine hearts before and after MLO-Y4 conditioned media (CM) was applied, and second by using EKG to measure cardiac parameters in live, anesthetized mice before, during, and after mechanical tibial loading. We found that CM caused arrhythmias in externally-paced hearts, while it caused an increase in contractility in self-paced hearts. We also found that tibia loading lead to an immediate decrease in heart rate and an improvement in heart rate variability in live anesthetized mice. Finally, we analyzed serum samples taken after loading and identified factors that were elevated in both male and female mice. One statistically elevated metabolite was present in all loaded groups. The atomic mass of the derivatized compound corresponded to the derivatized mass of acetic acid under the experimental conditions.

4.2 Bone Conditioned Media

We observed two different outcomes when we exposed hearts to MLOY4 conditioned media due to different experimental setups. In externally paced hearts, the SA nodes had been removed in order to give full pacing control to the intact, isolated heart. This is the simpler model of cardiac function to ensure that hearts beat at a consistent rate during experimentation. Interestingly, these hearts displayed arrhythmias upon exposure to bone CM. To better understand the mechanisms at work, a second round of experiments was performed in which the hearts retained the SA node and were allowed to self-pace. In these experiments a statistically significant increase in peak contractile force and total contractile force was observed after approximately 2 min of CM being added to the Langendorff bath. The increase in cardiac contractility observed when CM was applied to self-paced hearts would increase overall cardiac output *in vivo* since increased contractility reduces end systolic volume and Stroke Volume = End Diastolic Volume – End Systolic Volume and Cardiac Output = Stroke Volume x Heart Rate. It is possible that factors released by bone during may work to increase cardiac output in response to bone loading.

Our lab has previously performed work on MLO-Y4 conditioned media and found 10% CM increased *ex vivo* soleus muscle contractile force by 25% (Huang et al., 2017). In those previous experiments, CM was found to enhance caffeine-induced calcium release from sarcoplasmic reticulum, suggestion a possible mode of action for the increase in contractility. Changes in intracellular calcium handling may have also contributed to the arrhythmias during external pacing (Vassalle & Lin, 2004). The self-paced hearts were able to beat faster than the externally-paced hearts. It is possible that calcium had more time to build up in the externally-paced hearts, triggering an early depolarization (arrhythmia) prior to the next external

stimulation. This type of calcium mishandling is a well-established cause of cardiac arrhythmias (Dridi et al., 2020). It is likely that the bone conditioned media has more of an effect on the ventricular contractile myocytes than the SA or AV nodal cells as we did not observe a change in heart rate with CM compared to controls in the isolated, self-paced hearts.

4.3 Bone Loading

The long bones of the leg, such as the tibia, are subjected to particular strain during cardiovascular exercise activities such as running or other high impact exercises (Han et al., 2018). We used a model of *in vivo* loading to apply bone strain to the tibia in a manner that did not also activate skeletal muscle contraction, signaling, or stretching of the muscle. This model allowed us to monitor the effects of bone loading without additional confounding variables. Several studies have implicated bone in endocrine signaling during exercise. For example, osteocalcin levels of have been shown to double during aerobic exercise and osteocalcin is necessary for the adaption of skeletal myofibril metabolism to exercise (Mera et al., 2016). Thus, the potential for bone-conditioned media and bone-derived signaling factors to induce changes in the heart, exists. Our lab has shown that FGF23 induces cardiac arrhythmias and prolongs QTc (Graves et al., 2021), while many studies have shown that FGF23 is involved in long-term cardiac remodeling (Faul et al., 2011, Touchberry et al., 2013) and increased circulating FGF23 is used clinically as a non-traditional indicator of poor cardiac outcomes in CKD patients (Leifheit-Nestler & Haffner, 2018).

During tibia loading, we observed a transient decrease in heart rate and an increase in heart rate variability. This was somewhat surprising given our findings in isolated hearts when conditioned media was added and which lead to changes in cardiac behavior which would have

increased cardiac output. We have hypothesized two possibilities to explain the transient decrease in heart rate. First, tibial nerve stimulation can lead to vagal nerve (cranial nerve 10) activation which can lead to decreases in HR (McCredie, 2007). Based on the speed at which the heart rate reduction occurred, a neural reflex seems likely. It is also possible that a metabolite may be responsible which will be discussed later.

Along with the decrease in heart rate, we also observed an increased heart rate variability. Heart rate variability is a characteristic of cardiovascular exercise and, long-term, of cardiovascular fitness in individuals such as endurance athletes (Cygankiewicz & Zareba, 2013). Heart rate variability measures the ability of the heart to respond quickly to changing physiological demands for cardiac output and is greatly influenced by the autonomic nervous system. Typically, the larger the heart rate variability, the larger the influence of vagal tone (vagal output) to the heart (parasympathetic) or reduced sympathetic output or a combination of the two. These findings add strength to the possibility that a reduction in sympathetic tone or increased vagal tone was involved in the change in heart rate.

It is known that an increase in vagal output (or reduction in sympathetic output) increases bone density (Tamimi et al., 2021, Johnson & Wilson, 2018) therefore loading of the bone may trigger vagal output in order to signal bone anabolism. Nevertheless, the change in heart rate and heart rate variability was short lived. Thus, it seems of limited utility in physical activity unless this change occurs upon the start of every load throughout the day or is used to prime mechanisms for loading or exercise. More research will need to be conducted to understand this response.

4.4 Metabolomics

The LC/QToF MS of serum samples revealed a consistent elevation in serum acetate in both male and female loaded groups. The relationship between acetate and the heart is complex. The heart is exceptionally well suited to use acetate as a fuel source; expression of mitochondrial AceCS2, the enzyme which converts acetate into acetyl-CoA for use in the tricarboxylic acid cycle, is higher than in any other tissue (Jacob et al., 1997). When injected intraperitoneal, acetate reduced heart rate and mean arterial pressure in conscious, radiotelemetry-monitored live animals (Poll et al., 2021). The effect began within minutes and peaked in approximately 8 minutes. Atenolol, a selective beta-1 adrenergic receptor antagonist, and tyramine, an indirect sympathomimetic, were able to prevent this decrease in heart rate but not the decrease in mean arterial pressure. This indicated that the reduction in heart rate was caused by an inhibition of sympathetic nervous system, rather than activation of the parasympathetic system. This could be a potential mechanism by which we observed rapid changes in heart rate that may have mediated neurally. Interestingly, previous research has also demonstrated that acetate transiently inhibits the contraction of isolated cardiomyocytes by increasing calcium uptake by mitochondria, inhibiting systolic function and decreasing cell shortening after 2 minutes of exposure (Schooley et al., 2014). Some Langendorff experiments have shown a decrease in heart rate but to a lesser degree and after a longer exposure than when injected (Poll et al., 2021). Jacob et al., found that in a Langendorff apparatus, high concentrations of acetate impaired the ability of cardiac tissue to metabolize fatty acids, impairing cardiac function by impairing ATP production (Jacob et al., 1997). It is possible that acetate may be responsible for the transient decreases in heart rate or it is possible that acetate is simply a biproduct that we are seeing after 30 minutes of loading. The

role of acetate in the cardiovascular and potentially other organ responses to bone loading needs further investigation.

4.5 Significance

In our two series of experiments (*ex vivo* and *in vivo*) we observed seemingly contradictory responses. We observed a transient decrease in heart rate upon bone loading *in vivo* and a prolonged increase in contractility using bone conditioned media in *ex vivo* contractility experiments. Whether both of these responses occur as part of a protective or adaptive response to loading needs to be more thoroughly investigated. Nevertheless, whether through a neural or direct effect by an endocrine factor, the *in vivo* and *ex vivo* experiments indicate an ability of the skeletal system to very rapidly effect changes in the heart. This has implications in exercise as well as in traumatic injury when bones may be strained. There are also potential implications for those with low bone mass and/or low activity level. If lower bone mass correlates to fewer osteocytes and a lower level of circulating signaling factors, or if a low activity level correlates with less bone strain and a lower level of circulating signaling factors, cardiac responses may be adversely affected. Finally, acetic acid may be yet another factor in the complex relationship between bone and chronic heart and kidney conditions which needs further exploration.

4.6 Limitations

First, it is unclear how anesthesia affected the response to tibial loading, especially if the observed changes were due to a neuronal-based signaling axis. It would be necessary to compare our results with the results using conscious animals to determine what, if, difference this made.

Second, the source of circulating acetate is difficult to determine from our work. The primary physiological source of acetate is from the diet and fermentation in the gut, but acetate is also produced any time deacetylation takes place (Moffett et al., 2020). It is also unclear at this point whether acetate is a definitely a cause of our observations (decreased heart rate, etc.) or an unrelated biproduct of some adjacent process.

Third, CM was generated by applying fluid flow sheer stress to MLO-Y4 cells for two hours. Given how rapidly tibial loading affected anesthetized mice, the time sheer stress was applied to MLO-Y4 cell cultures may have produced different factors than tibial loading *in vivo*. It is entirely possible that a different set of cardio-relevant signaling factors are dominant in the conditioned media after two hours of fluid flow sheer stress than are dominant in the serum of live anesthetized mice after two minutes of tibial loading.

4.7 Future Directions

To point towards a potential mechanism for the observed changes, it would be useful to monitor intracellular calcium handling in isolated cardiomyocytes to determine if CM affects this. Additionally, a decrease in heart rate upon the initiation of tibia loading was reliably observed during tibia loading experiments, but this decrease was transient and recovered to near baseline before the loading sequence ended, at which point a blood sample was collected. Repeating the tibia loading experiment under various other conditions would shed further light on our findings. First, drawing a blood sample as soon as this heart rate decrease was detected and analyzing this sample would indicate what factors were present in the serum during the observed decrease in heart rate. Second, blocking nerve conduction through the tibial nerve, or vagal and sympathetic efferent nerves using either surgical or chemical methods and repeating

the tibial strain experiments would indicate what role these nerves have in heart rate reduction. Thirdly, injecting acetic acid into the circulation of anesthetized mice would determine if its role is causative of cardiac changes, or an unrelated result of tibial strain.

REFERENCE LIST

1. Batra, N., Kar, R., & Jiang, J. X. (2012). Gap junctions and hemichannels in signal transmission, function and development of bone. *Biochimica et Biophysica Acta*, *1818*(8), 1909–1918. https://doi.org/10.1016/j.bbamem.2011.09.01

2. Bellenger, C. R., Fuller, J. T., Thomson, R. L., Davison, K., Robertson, E. Y., & Buckley, J. D. (2016). Monitoring athletic training status through autonomic heart rate regulation: a systematic review and meta-analysis. *Sports Medicine (Auckland, N.Z.)*, *46*(10), 1461–1486. https://doi.org/10.1007/s40279-016-0484-2

3. Berger, J. M., Singh, P., Khrimian, L., Morgan, D. A., Chowdhury, S., Arteaga-Solis, E., Horvath, T. L., Domingos, A. I., Marsland, A. L., Yadav, V. K., Rahmouni, K., Gao, X. B., & Karsenty, G. (2019). Mediation of the acute stress response by the skeleton. *Cell Metabolism*, *30*(5), 890–902.e8. https://doi.org/10.1016/j.cmet.2019.08.012

4. Buenzli, P. R., & Sims, N. A. (2015). Quantifying the osteocyte network in the human skeleton. *Bone*, *75*, 144–150. https://doi.org/10.1016/j.bone.2015.02.016

5. Busse, B., Djonic, D., Milovanovic, P., Hahn, M., Püschel, K., Ritchie, R. O., Djuric, M., & Amling, M. (2010). Decrease in the osteocyte lacunar density accompanied by hypermineralized lacunar occlusion reveals failure and delay of remodeling in aged human bone. *Aging Cell*, *9*(6), 1065–1075. https://doi.org/10.1111/j.1474-9726.2010.00633.

6. Campos-Staffico, A. M., Freitas, W. M., Carvalho, L., Coelho-Filho, O. R., Nadruz, W., Jr, Oliveira, R. B., Sposito, A. C., & Brasilia Study on Healthy Aging and Brasilia Heart Study (2020). Lower bone mass is associated with subclinical atherosclerosis, endothelial dysfunction and carotid thickness in the very elderly. *Atherosclerosis*, *292*, 70–74. https://doi.org/10.1016/j.atherosclerosis.2019.11.007

7. Carpenter, K. A., & Ross, R. D. (2020). Sclerostin antibody treatment increases bone mass and normalizes circulating phosphate levels in growing hyp mice. *Journal Of Bone And Mineral Research : The Official Journal Of The American Society For Bone And Mineral Research*, *35*(3), 596–607. https://doi.org/10.1002/jbmr.3923

8. Chaible, L. M., Sanches, D. S., Cogliati, B., Mennecier, G., & Dagli, M. L. (2011). Delayed osteoblastic differentiation and bone development in Cx43 knockout mice. *Toxicologic Pathology*, *39*(7), 1046–1055. https://doi.org/10.1177/0192623311422075

9. Cygankiewicz, I., & Zareba, W. (2013). Heart rate variability. *Handbook of Clinical Neurology*, *117*, 379–393. https://doi.org/10.1016/B978-0-444-53491-0.00031-6

10. Delgado-Calle, J., Sato, A. Y., & Bellido, T. (2017). Role and mechanism of action of sclerostin in bone. *Bone*, *96*, 29–37. https://doi.org/10.1016/j.bone.2016.10.007

11. DeSaix, P and Johnson, E. (2013). *Anatomy and Physiology*. OpenStax. https://open.umn.edu/opentextbooks/textbooks/169

12. Diaz-Franco, M. C., Franco-Diaz de Leon, R., & Villafan-Bernal, J. R. (2019). Osteocalcin-GPRC6A: An update of its clinical and biological multi-organic interactions (Review). *Molecular Medicine Reports*, *19*(1), 15–22. https://doi.org/10.3892/mmr.2018.9627

13. Dridi, H., Kushnir, A., Zalk, R., Yuan, Q., Melville, Z., & Marks, A. R. (2020). Intracellular calcium leak in heart failure and atrial fibrillation: a unifying mechanism and therapeutic target. *Nature Reviews. Cardiology*, *17*(11), 732–747. https://doi.org/10.1038/s41569-020-0394-8

14. Ellies, D. L., Viviano, B., McCarthy, J., Rey, J. P., Itasaki, N., Saunders, S., & Krumlauf, R. (2006). Bone density ligand, Sclerostin, directly interacts with LRP5 but not LRP5G171V to modulate Wnt activity. *Journal Of Bone And Mineral Research : The Official Journal Of The American Society For Bone And Mineral Research*, *21*(11), 1738–1749. https://doi.org/10.1359/jbmr.060810

15. Faul, C., Amaral, A. P., Oskouei, B., Hu, M. C., Sloan, A., Isakova, T., Gutiérrez, O. M., Aguillon-Prada, R., Lincoln, J., Hare, J. M., Mundel, P., Morales, A., Scialla, J., Fischer, M., Soliman, E. Z., Chen, J., Go, A. S., Rosas, S. E., Nessel, L., Townsend, R. R., … Wolf, M. (2011). FGF23 induces left ventricular hypertrophy. *The Journal of Clinical Investigation*, *121*(11), 4393–4408. https://doi.org/10.1172/JCI46122

16. Felsenfeld, A. J., Levine, B. S., & Rodriguez, M. (2015). Pathophysiology of calcium, phosphorus, and magnesium dysregulation in chronic kidney disease. *Seminars in Dialysis*, *28*(6), 564–577. https://doi.org/10.1111/sdi.12411

17. Fohtung, R. B., Brown, D. L., Koh, W. J., Bartz, T. M., Carbone, L. D., Civitelli, R., Stein, P. K., Chaves, P. H., Kestenbaum, B. R., & Kizer, J. R. (2017). Bone mineral and risk of heart failure in older adults: the cardiovascular health study. *Journal of the American Heart Association*, *6*(3), e004344. https://doi.org/10.1161/JAHA.116.004344

18. Frost H. M. (1987). The mechanostat: a proposed pathogenic mechanism of osteoporoses and the bone mass effects of mechanical and nonmechanical agents. *Bone and Mineral*, *2*(2), 73–85

19. Gamie, Z., Korres, N., Leonidou, A., Gray, A. C., & Tsiridis, E. (2012). Sclerostin monoclonal antibodies on bone metabolism and fracture healing. *Expert Opinion on Investigational Drugs*, *21*(10), 1523–1534. https://doi.org/10.1517/13543784.2012.713936

20. Graves, J. M., J. A., Hamill, C. S., Wang, D., Ahuja, R., Patel, S., Faul, C., & Wacker, M. J. (2021). Fibroblast growth factor 23 (FGF23) induces ventricular arrhythmias and

prolongs QTc interval in mice in an FGF receptor 4-dependent manner. *American Journal of Physiology. Heart and Circulatory Physiology*, *320*(6), H2283–H2294. https://doi.org/10.1152/ajpheart.00798.2020

21. Gu, X., Xu, J., Zhu, L., Bryson, T., Yang, X. P., Peterson, E., & Harding, P. (2016). Prostaglandin E2 reduces cardiac contractility via EP3 receptor. *Circulation. Heart Failure*, *9*(8), 10.1161/CIRCHEARTFAILURE.116.003291 e003291. https://doi.org/10.1161/CIRCHEARTFAILURE.116.003291

22. Guntur, A. R., & Rosen, C. J. (2012). Bone as an endocrine organ. *Endocrine Practice: Official Journal of The American College of Endocrinology and the American Association of Clinical Endocrinologists*, *18*(5), 758–762. https://doi.org/10.4158/EP12141.RA

23. Han, Y., You, X., Xing, W., Zhang, Z., & Zou, W. (2018). Paracrine and endocrine actions of bone-the functions of secretory proteins from osteoblasts, osteocytes, and osteoclasts. *Bone Research*, *6*, 16. https://doi.org/10.1038/s41413-018-0019-6

24. Hiam, D., Voisin, S., Yan, X., Landen, S., Jacques, M., Papadimitriou, I. D., Munson, F., Byrnes, E., Brennan-Speranza, T. C., Levinger, I., & Eynon, N. (2019). The association between bone mineral density gene variants and osteocalcin at baseline, and in response to exercise: The Gene SMART study. *Bone*, *123*, 23–27. https://doi.org/10.1016/j.bone.2019.03.015

25. Huang, J., Romero-Suarez, S., Lara, N., Mo, C., Kaja, S., Brotto, L., Dallas, S. L., Johnson, M. L., Jähn, K., Bonewald, L. F., & Brotto, M. (2017). Crosstalk between MLO-Y4 osteocytes and C2C12 muscle cells is mediated by the Wnt/β-catenin pathway. *JBMR Plus*, *1*(2), 86–100. https://doi.org/10.1002/jbm4.10015

26. Jacob, A. D., Elkins, N., Reiss, O. K., Chan, L., & Shapiro, J. I. (1997). Effects of acetate on energy metabolism and function in the isolated perfused rat heart. *Kidney International*, *52*(3), 755–760. https://doi.org/10.1038/ki.1997.392

27. Ji, Y. Q., Guan, L. N., Yu, S. X., Yin, P. Y., Shen, X. Q., Sun, Z. W., Liu, J., Lv, W., Yu, G. P., & Ren, C. (2018). Serum sclerostin as a potential novel biomarker for heart valve calcification in patients with chronic kidney disease. *European Review for Medical and Pharmacological Sciences*, *22*(24), 8822–8829. https://doi.org/10.26355/eurrev_201812_16650

28. Jiang, J. X., Siller-Jackson, A. J., & Burra, S. (2007). Roles of gap junctions and hemichannels in bone cell functions and in signal transmission of mechanical stress. *Frontiers in Bioscience : A Journal and Virtual Library*, *12*, 1450–1462. https://doi.org/10.2741/2159Jilka & O'Brien, 2016

29. Johnson, R. L., & Wilson, C. G. (2018). A review of vagus nerve stimulation as a therapeutic intervention. *Journal of Inflammation Research*, *11*, 203–213. https://doi.org/10.2147/JIR.S163248

30. Kamińska, J., Stopiński, M., Mucha, K., Pac, M., Gołębiowski, M., Niewczas, M. A., Pączek, L., & Foroncewicz, B. (2021). Circulating osteoprotegerin in chronic kidney disease and all-cause mortality. *International Journal of General Medicine*, *14*, 2413–2420. https://doi.org/10.2147/IJGM.S302251

31. Kao, Y. H., Chen, Y. C., Lin, Y. K., Shiu, R. J., Chao, T. F., Chen, S. A., & Chen, Y. J. (2014). FGF-23 dysregulates calcium homeostasis and electrophysiological properties in HL-1 atrial cells. *European Journal of Clinical Investigation*, *44*(8), 795–801. https://doi.org/10.1111/eci.12296

32. Karner, C. M., & Long, F. (2018). Glucose metabolism in bone. *Bone*, *115*, 2–7. https://doi.org/10.1016/j.bone.2017.08.008

33. Kouvelioti, R., Kurgan, N., Falk, B., Ward, W. E., Josse, A. R., & Klentrou, P. (2019). Cytokine and Sclerostin response to high-intensity interval running versus cycling. *Medicine and Science in Sports and Exercise*, *51*(12), 2458–2464.

34. Leifheit-Nestler, M., & Haffner, D. (2018). Paracrine effects of FGF23 on the heart. *Frontiers in Endocrinology*, *9*, 278. https://doi.org/10.3389/fendo.2018.00278

35. Liu, S., Gao, F., Wen, L., Ouyang, M., Wang, Y., Wang, Q., Luo, L., & Jian, Z. (2017). Osteocalcin induces proliferation via positive activation of the PI3K/AKT, P38 MAPK pathways and promotes differentiation through activation of the GPCR6A-ERK1/2 pathway in C2C12 myoblast cells. *Cellular Physiology and Biochemistry : International Journal of Experimental Cellular Physiology, Biochemistry, and Pharmacology*, *43*(3), 1100–1112. https://doi.org/10.1159/000481752

36. Lombardi, G., Corsetti, R., Lanteri, P., Grasso, D., Vianello, E., Marazzi, M. G., Graziani, R., Colombini, A., Galliera, E., Corsi Romanelli, M. M., & Banfi, G. (2014). Reciprocal regulation of calcium-/phosphate-regulating hormones in cyclists during the Giro d'Italia 3-week stage race. *Scandinavian Journal of Medicine & Science in Sports*, *24*(5), 779–787. https://doi.org/10.1111/sms.12080

37. Ma, Y., Yue, Z., Zhang, B., Yang, M., Lao, H., Lai, W., Zeng, Y., Chen, S., & Liu, P. (2018). Calcium signal pathway is involved in prostaglandin E2 induced cardiac fibrosis in cardiac fibroblasts. *Journal of Pharmacy & Pharmaceutical Sciences : A Publication of the Canadian Society for Pharmaceutical Sciences, Societe Canadienne des Sciences Pharmaceutiques*, *21*(1), 326–339. https://doi.org/10.18433/jpps29322

38. McCredie J. (2007). Nerves in bone: the silent partners. *Skeletal Radiology*, *36*(6), 473–475. https://doi.org/10.1007/s00256-006-0253-7

39. Mera, P., Laue, K., Ferron, M., Confavreux, C., Wei, J., Galán-Díez, M., Lacampagne, A., Mitchell, S. J., Mattison, J. A., Chen, Y., Bacchetta, J., Szulc, P., Kitsis, R. N., de Cabo, R., Friedman, R. A., Torsitano, C., McGraw, T. E., Puchowicz, M., Kurland, I., & Karsenty, G. (2016). Signaling in myofibers is necessary and sufficient for optimum adaptation to exercise. *Cell Metabolism*, *23*(6), 1078–1092. https://doi.org/10.1016/j.cmet.2016.05.004

40. Mizokami, A., Kawakubo-Yasukochi, T., & Hirata, M. (2017). Osteocalcin and its endocrine functions. *Biochemical Pharmacology*, *132*, 1–8. https://doi.org/10.1016/j.bcp.2017.02.001

41. Mo, C., Romero-Suarez, S., Bonewald, L., Johnson, M., & Brotto, M. (2012). Prostaglandin E2: from clinical applications to its potential role in bone- muscle crosstalk and myogenic differentiation. *Recent Patents on Biotechnology*, *6*(3), 223–229. https://doi.org/10.2174/1872208311206030223

42. Moffett, J. R., Puthillathu, N., Vengilote, R., Jaworski, D. M., & Namboodiri, A. M. (2020). Acetate revisited: A key biomolecule at the nexus of metabolism, epigenetics and oncogenesis-part 1: acetyl-coA, acetogenesis and acyl-coA short-chain synthetases. *Frontiers in Physiology*, *11*, 580167.https://doi.org/10.3389/fphys.2020.580167

43. Moser, S. C., & van der Eerden, B. (2019). Osteocalcin-a versatile bone-derived hormone. *Frontiers in Endocrinology*, *9*, 794. https://doi.org/10.3389/fendo.2018.00794

44. Phillips, J. A., Almeida, E. A., Hill, E. L., Aguirre, J. I., Rivera, M. F., Nachbandi, I., Wronski, T. J., van der Meulen, M. C., & Globus, R. K. (2008). Role for beta1 integrins in cortical osteocytes during acute musculoskeletal disuse. *Matrix Biology: Journal of the International Society for Matrix Biology*, *27*(7), 609–618. https://doi.org/10.1016/j.matbio.2008.05.003

45. Poelzl, G., Trenkler, C., Kliebhan, J., Wuertinger, P., Seger, C., Kaser, S., Mayer, G., Pirklbauer, M., Ulmer, H., & Griesmacher, A. (2014). FGF23 is associated with disease severity and prognosis in chronic heart failure. *European Journal of Clinical Investigation*, *44*(12), 1150–1158. https://doi.org/10.1111/eci.12349

46. Poll, B. G., Xu, J., Jun, S., Sanchez, J., Zaidman, N. A., He, X., Lester, L., Berkowitz, D. E., Paolocci, N., Gao, W. D., & Pluznick, J. L. (2021). Acetate, a short-chain fatty acid, acutely lowers heart rate and cardiac contractility along with blood pressure. *The Journal of Pharmacology and Experimental Therapeutics*, *377*(1), 39–50. https://doi.org/10.1124/jpet.120.000187

47. Qi, Z., Liu, W., & Lu, J. (2016). The mechanisms underlying the beneficial effects of exercise on bone remodeling: Roles of bone-derived cytokines and microRNAs. *Progress in Biophysics and Molecular Biology*, *122*(2), 131–139. https://doi.org/10.1016/j.pbiomolbio.2016.05.010

48. Richter, B., & Faul, C. (2018). FGF23 actions on target tissues-with and without Klotho. *Frontiers in Endocrinology*, *9*, 189. https://doi.org/10.3389/fendo.2018.00189

49. Robling, A. G., & Bonewald, L. F. (2020). The osteocyte: new insights. *Annual Review of Physiology*, *82*, 485–506. https://doi.org/10.1146/annurev-physiol-021119-034332

50. Schooley, J. F., Namboodiri, A. M., Cox, R. T., Bünger, R., & Flagg, T. P. (2014). Acetate transiently inhibits myocardial contraction by increasing mitochondrial calcium uptake. *BMC Physiology*, *14*, 12. https://doi.org/10.1186/s12899-014-0012-2

51. St John, H. C., Hansen, S. J., & Pike, J. W. (2016). Analysis of SOST expression using large minigenes reveals the MEF2C binding site in the evolutionarily conserved region (ECR5) enhancer mediates forskolin, but not 1,25-dihydroxyvitamin D_3 or β_1 responsiveness. *The Journal of Steroid Biochemistry and Molecular Biology*, *164*, 277–280. https://doi.org/10.1016/j.jsbmb.2015.09.005

52. Stavrinou, E., Sarafidis, P. A., Koumaras, C., Loutradis, C., Giamalis, P., Tziomalos, K., Karagiannis, A., & Papagianni, A. (2019). Increased sclerostin, but not dickkopf-1 protein, is associated with elevated pulse wave velocity in hemodialysis subjects. *Kidney & Blood Pressure Research*, *44*(4), 679–689. https://doi.org/10.1159/000501205

53. Sutherland, F. J., Shattock, M. J., Baker, K. E., & Hearse, D. J. (2003). Mouse isolated perfused heart: characteristics and cautions. *Clinical and Experimental Pharmacology & Physiology*, *30*(11), 867–878. https://doi.org/10.1046/j.1440-1681.2003.03925.

54. Tacey, A., Qaradakhi, T., Brennan-Speranza, T., Hayes, A., Zulli, A., & Levinger, I. (2018). Potential role for osteocalcin in the development of atherosclerosis and blood vessel disease. *Nutrients*, *10*(10), 1426. https://doi.org/10.3390/nu10101426

55. Tamimi, A., Tamimi, F., Juweid, M., Al-Qudah, A. A., Al Masri, A., Dahbour, S., Al Bahou, Y., Shareef, A., & Tamimi, I. (2021). Could vagus nerve stimulation influence bone remodeling?. *Journal of Musculoskeletal & Neuronal Interactions*, *21*(2), 255–262.

56. Tatsumi, S., Ishii, K., Amizuka, N., Li, M., Kobayashi, T., Kohno, K., Ito, M., Takeshita, S., & Ikeda, K. (2007). Targeted ablation of osteocytes induces osteoporosis with defective mechanotransduction. *Cell Metabolism*, *5*(6), 464–475. https://doi.org/10.1016/j.cmet.2007.05.001

57. Touchberry, C. D., Green, T. M., Tchikrizov, V., Mannix, J. E., Mao, T. F., Carney, B. W., Girgis, M., Vincent, R. J., Wetmore, L. A., Dawn, B., Bonewald, L. F., Stubbs, J. R., & Wacker, M. J. (2013). FGF23 is a novel regulator of intracellular calcium and cardiac contractility in addition to cardiac hypertrophy. *American Journal of Physiology. Endocrinology and Metabolism*, *304*(8), E863–E873. https://doi.org/10.1152/ajpendo.00596.2012

58. Vassalle, M., & Lin, C. I. (2004). Calcium overload and cardiac function. *Journal of Biomedical Science*, *11*(5), 542–565. https://doi.org/10.1007/BF02256119

59. Vaughan, T. J., Mullen, C. A., Verbruggen, S. W., & McNamara, L. M. (2015). Bone cell mechanosensation of fluid flow stimulation: a fluid-structure interaction model characterising the role integrin attachments and primary cilia. *Biomechanics and Modeling in Mechanobiology*, *14*(4), 703–718. https://doi.org/10.1007/s10237-014-0631-3Vogt, et al, 2019

60. von Jeinsen, B., Sopova, K., Palapies, L., Leistner, D. M., Fichtlscherer, S., Seeger, F. H., Honold, J., Dimmeler, S., Aßmus, B., Zeiher, A. M., & Keller, T. (2019). Bone marrow and plasma FGF-23 in heart failure patients: novel insights into the heart-bone axis. *ESC Heart Failure*, *6*(3), 536–544. https://doi.org/10.1002/ehf2.12416

61. Wacker, M. J., Touchberry, C. D., Silswal, N., Brotto, L., Elmore, C. J., Bonewald, L. F., Andresen, J., & Brotto, M. (2016). Skeletal muscle, but not cardiovascular function, is altered in a mouse model of autosomal recessive hypophosphatemic rickets. *Frontiers in Physiology*, *7*, 173. https://doi.org/10.3389/fphys.2016.00173

62. Wang, H., Sun, W., Ma, J., Pan, Y., Wang, L., & Zhang, W. (2014). Polycystin-1 mediates mechanical strain-induced osteoblastic mechanoresponses via potentiation of intracellular calcium and Akt/β-catenin pathway. *PloS One*, *9*(3), e91730. https://doi.org/10.1371/journal.pone.0091730

63. Wehrens, X. H., Kirchhoff, S., & Doevendans, P. A. (2000). Mouse electrocardiography: an interval of thirty years. *Cardiovascular Research*, *45*(1), 231–237. https://doi.org/10.1016/s0008-6363(99)00335-1

64. Xia, X., Batra, N., Shi, Q., Bonewald, L. F., Sprague, E., & Jiang, J. X. (2010). Prostaglandin promotion of osteocyte gap junction function through transcriptional regulation of connexin 43 by glycogen synthase kinase 3/beta-catenin signaling. *Molecular and Cellular Biology*, *30*(1), 206–219. https://doi.org/10.1128/MCB.01844-08

65. Xu, H., Zhang, J., Wu, J., Guan, Y., Weng, Y., & Shang, P. (2012). Oscillatory fluid flow elicits changes in morphology, cytoskeleton and integrin-associated molecules in MLO-Y4 cells, but not in MC3T3-E1 cells. *Biological Research*, *45*(2), 163–169. https://doi.org/10.4067/S0716-97602012000200008

66. Yan, Y., Wang, L., Ge, L., & Pathak, J. L. (2020). Osteocyte-mediated translation of mechanical stimuli to cellular signaling and its role in bone and non-bone-related clinical complications. *Current Osteoporosis Reports*, *18*(1), 67–80. https://doi.org/10.1007/s11914-020-00564-9

67. Zhang, M., Yan, J., Zhu, M., & Ni, Z. (2015). Fibroblast growth factor 23 predicts coronary calcification and poor prognosis in patients with chronic kidney disease stages 3-5D. *Annals of Clinical and Laboratory Science*, *45*(1), 17–22

68. Zhang, Y., Qi, L., Gu, W., Yan, Q., Dai, M., Shi, J., Zhai, Y., Chen, Y., Liu, J., Wang, W., Ning, G., & Hong, J. (2010). Relation of serum osteocalcin level to risk of coronary heart disease in Chinese adults. *The American Journal of Cardiology*, *106*(10), 1461–1465.

VITA

Mark A Gray was born in Bentonville, Arkansas on January 24th, 1991, and grew up in Powel, Missouri. He received a High School Diploma from Bob Jones Academy of Home Education in 2011. He attended Crowder Community College in Neosho Missouri, Cox College of Nursing in Springfield, Missouri, and received his Dual B.S. in Chemistry and Biomedical Science from the University of Missouri in the spring of 2018 after working on a variety of research projects in both majors. In the fall of 2018, he enrolled in the graduate school at the University of Missouri-Kansas City. He joined the Wacker lab where he participated in research on the effect of bone strain on cardiac function. He also worked on a variety of medical research projects with Dr. Gary Sutkin's Surgical Innovation Lab. Since the summer of 2020, Mark has resided in Manhattan, Kansas where he has been a full-time researcher, first in the lab of Dr. Zhilong Yang, specializing in poxvirus-host cell metabolic interactions and of late in the Molecular R&D department of the Kansas State University Veterinary Diagnostic Lab where he designs and validates novel qPCR and Sanger-sequence assays for veterinary clinicians. He will start medical school at the University of Kansas in the summer of 2022 and attend the Salina, KS campus where he plans to take a special interest in the health of migrants and immigrants and in logistical models of healthcare delivery, especially in poor, rural, and indigenous-administered regions; that, or space-medicine.